widely prescribed to lower cholesterol level in patients. Numerous studies, however, suggest that statin therapy has additional cardiovascular protective effects that may function independently of their ability to lower serum cholesterol levels (1, 2). These cholesterol-independent or pleiotropic effects of statins involve improving endothelial function, decreasing oxidative stress and inflammation, inhibiting the thrombogenic response, and enhancing the stability of atherosclerotic plaques (3, 4). Recent evidence suggests that most of these effects are mediated by the inhibitory effect of statins on isoprenoid synthesis and by activation of statin on phosphatidylinositol 3-kinase (PI3K)/Akt pathway (5 – 7). Some reports showed that a clinically relevant dose of statins activate Akt (8, 9). However, the molecular mechanism of pleiotropic effects via Akt remains unclear. Akt is critical for the regulation of vascular endothelial functions and maintenance of vascular integrity (10, 11). The Akt-driven signaling network is capable of regulating cellular processes by modulating transcription and translation and by modifying proteins at the post-translational level. Kureishi et al. demonstrated that Akt activation by statins then inhibits apoptosis, acutely increases nitric oxide (NO) production, activates migration, and promotes angiogenesis (12). These effects of statins were prevented by PI3K inhibitors or the dominant negative form of Akt (12). Although many studies have reported that these effects depend on endothelial NO synthase (eNOS) activation via Akt, it is impossible to explain them by only eNOS activation (13, 14). Indeed, each physiological response downstream of Akt appears to be mediated by multiple targets. In fact, a careful search of the literature finds over 100 reported non-redundant Akt substrates, and each signaling pathway is activated (15). Due to the complexity of Akt involvement in various cellular processes, the downstream effectors of Akt that are the most critical to the physiological roles of Akt remain to be determined. It is important to understand the nature and molecular mechanism of statin-induced Akt activation because it may provide novel insights about the regulatory control of endothelial cell function and lead to the identification of new pharmacological targets.

Here, we attempted to perform affinity purification and proteomic analysis to elucidate the role of Akt signaling in the pleiotropic effects of statin. Affinity purification strategies employing epitope tags and physiological conditions have proven to be effective for targeted protein interactions mapping efforts.

2. Methods

The mapping of protein-protein interactions has matured for a few years through significant technology developments and methods standardization. Therefore, the identification of protein interaction partners has become a standard assay in numerous laboratories. In interaction research, several approaches have been developed for purifying and identifying protein complexes, including two-hybrid methods (16), enzyme assays (17), or tandem affinity purification (TAP) of protein complexes followed by mass spectrometric analysis (18, 19). The data from these experiments contain many false positives and false negatives, but these methods provide beneficial information about protein-protein relationships and protein function. These approaches can be applicable to disease-related signaling pathways. Accordingly, to establish a more systematic methodology for these studies, new and efficient proteome technologies are required. In this study, we present an effective method for the identification of multi-protein complexes in rat aortic endothelial cells (rAECs).

We explored the use of strep-tag method for the isolation of Akt1 complexes from rAECs. This protein purification system has previously been shown to allow the rapid, single-step purification of recombinant proteins from mammalian cellular lysates (20 – 22). Strep-tag is an eight amino acid peptide that has strong binding affinity for an engineered streptavidin derivative called strep-Tactin (20, 23). Our method involved the fusion of the strep-tag to Akt1 and introduction of the construct into the rAECs by adenoviral vectors. The cells were maintaining the expression of strep-tagged Akt1 and stimulated by pravastatin or pitavastatin for 10 min because Western blotting showed rapid phosphorylation of Akt1 at S473 and T308 at 10 min, a peak by pravastatin stimulation. Lysates expressing the strep-tagged Akt1 were then passed through a strep-Tactin column and bound proteins were specifically eluted using a derivative of biotin called desthiobiotin under physiological conditions. The purified protein assemblies were separated by denaturing gel electrophoresis, and individual bands were digested by trypsin, analyzed by matrix-assisted laser desorption/ionization-time-of-flight mass spectrometry (MALDI-TOF MS), and identified by database search algorithms (24) (Fig. 1)

3. Results and Discussion

Using this technique, the bait protein, Akt, and their 23 interaction partners were systematically purified and identified. Some of these proteins have known cellular functions and they encompass many signaling pathways. These included enzymes, such as protein kinases; translational regulators; cytoskeletal proteins; and hypo-

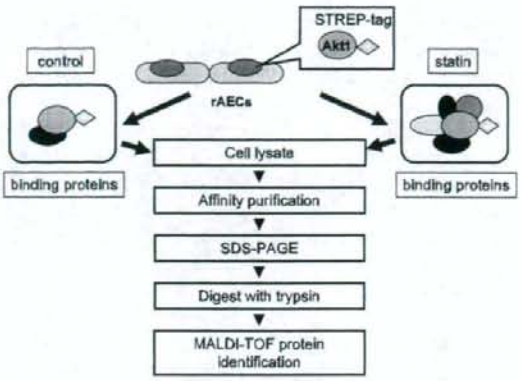

Fig. 1. Schematic overview of the strep-tag purification coupled to MS analysis.

thetical proteins. The identified interactions with Akt involved several known interactions and few previous reported interactions. In addition, we found 14 or 6 candidate proteins that up- or down- regulated the binding after 10 min of statin stimulation, respectively. The wide range of different proteins involved suggests that statin has profound effects on the biomolecular response and physiological consequence of vascular endothelium functions. However it is necessary to validate the specificity of each interaction because some of these results may be false positives. Some examples of the Akt1-associated molecules identified are as follows:

3.1. Hsp90

NO signaling is important in statin-mediated endothelial function (12). A number of studies have revealed that statins may increase eNOS activity via post-translation activation of the PI3K/Akt pathway (8, 12). In the present study, however, we could not detect the binding of eNOS to Akt1 under statin stimulation. This result suggests that eNOS engagements by Akt1 are weak or this is an indirect association. Instead, we identified the molecular chaperone heat-shock protein 90 (Hsp90) as Akt1-binding protein. Brouet et al. reported that statin-induced eNOS activation via Akt was through an interaction with Hsp90 (25). Moreover, Sato et al. reported that Akt interacts with Hsp90 on stimulation and this interaction enhances Akt enzymatic activity (26), suggesting that Hsp90 may serve as a scaffold protein for the efficient phosphorylation of eNOS by Akt (25, 27, 28). Taken together, the interaction between Akt1 and Hsp90 that we observed might be related to control eNOS activation.

3.2. mTOR/S6K

We found an association between Akt1 and the mammalian target of rapamycin (mTOR), which is already identified as substrate of Akt. Furthermore, we validated the specificity of this interaction by immunoprecipitation with endogenous proteins. The serine /threonine kinase mTOR is one of the most important downstream targets of PI3K/Akt. mTOR signaling has been demonstrated to be involved in the control of cell growth and proliferation (29). S6K plays a role in regulating the translation machinery and is controlled by mTOR, an immediate downstream effector of Akt (30). We analyzed activation of S6K to validate the mTOR/S6K pathway. Western blot analysis showed that pravastatin induced the phosphorylation of S6K on T389, thereby leading to enzyme activation. Pretreatment of cells with LY294002, a PI3K inhibitor, abolished the phosphorylation of Akt and S6K, whereas pretreatment with rapamycin, an mTOR inhibitor, inhibited only S6K phosphorylation. These data indicated that pravastatin activated the PI3K/Akt /mTOR/S6K pathway in this sequential manner in rAECs. Furthermore, rapamycin depressed pravastatin-induced rAEC proliferation. Nevertheless, the mTOR pathway contributed little to in vitro tube formation.

3.3. Cytoskeletal proteins

We identified several cytoskeletal proteins, non-muscle alpha-actinin 1, vimentin, and beta-actin, as Akt1 binding proteins. Furthermore, we confirmed endogenous binding of some of these proteins by immunoprecipitation. Confocal microscopic analysis also revealed that endogenous Akt rapidly translocated to perikaryon and cytoplasm from the nucleus by pravastatin stimulation. Akt translocation to the cytoplasm by statin stimulation seemed to be related to the interaction of Akt1 with the cytoskeletal proteins. Skaletz-Rorowski et al. has shown that Akt rapidly translocated to discrete sites at membrane ruffles in the simvastatin-treated endothelial cells (31). Their results agree with our results from mass spectrometric analysis, validating the confocal microscopic analysis. Cellular movement requires the reorganization of the actin cytoskeleton and distinct patterns of actin reorganization. This is required as cells establish a leading edge and then generate contractile force to migrate forward (32). It has been shown that Akt transiently localized to the leading edge membrane of migratory cells in a PI3K-dependent manner (33, 34). Recently, Enomoto et al. identified an Akt substrate, designated Girdin/APE, which is an actin binding protein (35). Akt phosphorylated Girdin accumulates at the leading edge of migrating cells. Thus, Akt seems to be important for regulation

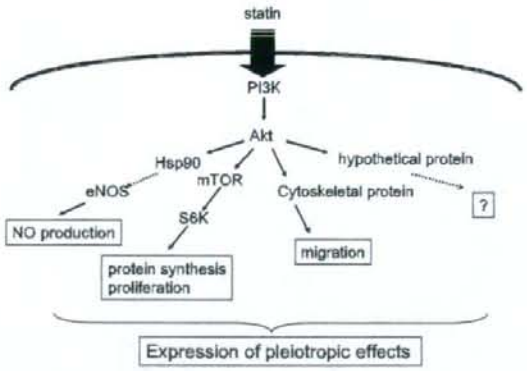

Fig. 2. Schematic representation of the proposed molecular mechanisms activated by statins in endothelial cells and responsible for pleiotropic effects.

of cell migration via actin reorganization (36) and through phosphorylation of the cytoskeletal protein Girdin. These data suggest that thanslocation of Akt1 and binding with cytoskeletal proteins of Akt1 participate in migration.

Taken together, statin induced activation of the PI3K/Akt pathway was shown to active many effectors and play an important role in mediating NO production, proliferation, and migrations in ECs (10, 37) (Fig. 2).

4. Conclusions

Identification of protein complexes is the key to understanding cellular functions including the transduction of inter- and/or intra-cellular signals and the regulation of gene expression. Aberrant protein-protein interactions are implicated in a number of diseases; therefore the study of protein complexes is the object of significant research in pharmacology. Furthermore, the information gained from protein interaction studies will ultimately lead to the discovery of novel pathway associations and therapeutic targets.

In this study, we have introduced a method for identifying protein-protein interactions using affinity purification and MS-based protein identification. We demonstrated that the strep method is very effective for purifying and identification of associated protein complexes. We tried to clarify the molecular mechanisms of the pleiotropic effects of statin with this method. Furthermore, we have identified many known interactions and several unreported proteins and hypothetical proteins to be Akt-binding proteins. As a result, it was revealed that statins activate not only the eNOS pathway but also many other pathways via Akt. Thus, the clarification of mechanisms for the pleiotropic effects of statins may lead to a better understanding of EC functions and provide avenues for the development of novel therapeutic interventions.

The simplicity and convenience of the single-step strep method, as well as its reliability and efficacy, would also make it useful for high-throughput applications both in academic research and in industrial drug development projects. The methodology presented here provides a new tool for proteomics in post-genomic medicinal science.

Acknowledgments

We thank Dr. Y. Funae (Osaka City University) for discussions and comments on the manuscript. The authors also thank Ms. Azusa Inagaki for excellent technical assistance. This work was supported in part by Grants-in-Aid for Scientific Research (17390068, 19790389) from the Ministry of Education, Culture, Sports, Science, and Technology, Japan.

References

1 Influence of pravastatin and plasma lipids on clinical events in the West of Scotland Coronary Prevention Study (WOSCOPS). Circulation. 1998;97:1440–1445.
2 Liao JK. Clinical implications for statin pleiotropy. Curr Opin Lipidol. 2005;16:624–629.
3 Wolfrum S, Jensen KS, Liao JK. Endothelium-dependent effects of statins. Arterioscler Thromb Vasc Biol. 2003;23:729–736.
4 Walter DH, Dimmeler S, Zeiher AM. Effects of statins on endothelium and endothelial progenitor cell recruitment. Semin Vasc Med. 2004;4:385–393.
5 Takemoto M, Liao JK. Pleiotropic effects of 3-hydroxy-3-methylglutaryl coenzyme a reductase inhibitors. Arterioscler Thromb Vasc Biol. 2001;21:1712–1719.
6 Endres M, Laufs U. Effects of statins on endothelium and signaling mechanisms. Stroke. 2004;35:2708–2711.
7 Cordle A, Koenigsknecht-Talboo J, Wilkinson B, Limpert A, Landreth G. Mechanisms of statin-mediated inhibition of small G-protein function. J Biol Chem. 2005;280:34202–34209.
8 Urbich C, Dernbach E, Zeiher AM, Dimmeler S. Double-edged role of statins in angiogenesis signaling. Circ Res. 2002;90:737–744.
9 Skaletz-Rorowski A, Walsh K. Statin therapy and angiogenesis. Curr Opin Lipidol. 2003;14:599–603.
10 Somanath PR, Razorenova OV, Chen J, Byzova TV. Akt1 in endothelial cell and angiogenesis. Cell Cycle. 2006;5:512–518.
11 Chen J, Somanath PR, Razorenova O, Chen WS, Hay N, Bornstein P, et al. Akt1 regulates pathological angiogenesis, vascular maturation and permeability in vivo. Nat Med. 2005; 11:1188–1196.
12 Kureishi Y, Luo Z, Shiojima I, Bialik A, Fulton D, Lefer DJ, et al. The HMG-CoA reductase inhibitor simvastatin activates the protein kinase Akt and promotes angiogenesis in normocholesterolemic animals. Nat Med. 2000;6:1004–1010.

13 Harris MB, Blackstone MA, Sood SG, Li C, Goolsby JM, Venema VJ, et al. Acute activation and phosphorylation of endothelial nitric oxide synthase by HMG-CoA reductase inhibitors. Am J Physiol Heart Circ Physiol. 2004;287:H560–H566.
14 Sata M, Nishimatsu H, Suzuki E, Sugiura S, Yoshizumi M, Ouchi Y, et al. Endothelial nitric oxide synthase is essential for the HMG-CoA reductase inhibitor cerivastatin to promote collateral growth in response to ischemia. FASEB J. 2001;15: 2530–2532.
15 Manning BD, Cantley LC. AKT/PKB signaling: navigating downstream. Cell. 2007;129:1261–1274.
16 Ito T, Chiba T, Ozawa R, Yoshida M, Hattori M, Sakaki Y. A comprehensive two-hybrid analysis to explore the yeast protein interactome. Proc Natl Acad Sci U S A. 2001;98:4569–4574.
17 Wehrman T, Kleaveland B, Her JH, Balint RF, Blau HM. Protein-protein interactions monitored in mammalian cells via complementation of beta-lactamase enzyme fragments. Proc Natl Acad Sci U S A. 2002;99:3469–3474.
18 Rigaut G, Shevchenko A, Rutz B, Wilm M, Mann M, Seraphin B. A generic protein purification method for protein complex characterization and proteome exploration. Nat Biotechnol. 1999;17:1030–1032.
19 Gavin AC, Bosche M, Krause R, Grandi P, Marzioch M, Bauer A, et al. Functional organization of the yeast proteome by systematic analysis of protein complexes. Nature. 2002;415: 141–147.
20 Skerra A, Schmidt TG. Use of the Strep-Tag and streptavidin for detection and purification of recombinant proteins. Methods Enzymol. 2000;326:271–304.
21 Junttila MR, Saarinen S, Schmidt T, Kast J, Westermarck J. Single-step Strep-tag purification for the isolation and identification of protein complexes from mammalian cells. Proteomics. 2005;5:1199–1203.
22 Vasilescu J, Figeys D. Mapping protein-protein interactions by mass spectrometry. Curr Opin Biotechnol. 2006;17:394–399.
23 Schmidt TG, Koepke J, Frank R, Skerra A. Molecular interaction between the Strep-tag affinity peptide and its cognate target, streptavidin. J Mol Biol. 1996;255:753–766.
24 Pandey A, Mann M. Proteomics to study genes and genomes. Nature. 2000;405:837–846.
25 Brouet A, Sonveaux P, Dessy C, Moniotte S, Balligand JL, Feron O. Hsp90 and caveolin are key targets for the proangiogenic nitric oxide-mediated effects of statins. Circ Res. 2001; 89:866–873.
26 Sato S, Fujita N, Tsuruo T. Modulation of Akt kinase activity by binding to Hsp90. Proc Natl Acad Sci U S A. 2000;97:10832–10837.
27 Brouet A, Sonveaux P, Dessy C, Balligand JL, Feron O. Hsp90 ensures the transition from the early Ca2+-dependent to the late phosphorylation-dependent activation of the endothelial nitric-oxide synthase in vascular endothelial growth factor-exposed endothelial cells. J Biol Chem. 2001;276:32663–32669.
28 Fontana J, Fulton D, Chen Y, Fairchild TA, McCabe TJ, Fujita N, et al. Domain mapping studies reveal that the M domain of hsp90 serves as a molecular scaffold to regulate Akt-dependent phosphorylation of endothelial nitric oxide synthase and NO release. Circ Res. 2002;90:866–873.
29 Sarbassov DD, Ali SM, Sabatini DM. Growing roles for the mTOR pathway. Curr Opin Cell Biol. 2005;17:596–603.
30 Fingar DC, Blenis J. Target of rapamycin (TOR): an integrator of nutrient and growth factor signals and coordinator of cell growth and cell cycle progression. Oncogene. 2004;23:3151–3171.
31 Skaletz-Rorowski A, Lutchman M, Kureishi Y, Lefer DJ, Faust JR, Walsh K. HMG-CoA reductase inhibitors promote cholesterol-dependent Akt/PKB translocation to membrane domains in endothelial cells. Cardiovasc Res. 2003;57:253–264.
32 Lauffenburger DA, Horwitz AF. Cell migration: a physically integrated molecular process. Cell. 1996;84:359–369.
33 Meili R, Ellsworth C, Lee S, Reddy TB, Ma H, Firtel RA. Chemoattractant-mediated transient activation and membrane localization of Akt/PKB is required for efficient chemotaxis to cAMP in Dictyostelium. Embo J. 1999;18:2092–2105.
34 Servant G, Weiner OD, Herzmark P, Balla T, Sedat JW, Bourne HR. Polarization of chemoattractant receptor signaling during neutrophil chemotaxis. Science. 2000;287:1037–1040.
35 Enomoto A, Murakami H, Asai N, Morone N, Watanabe T, Kawai K, et al. Akt/PKB regulates actin organization and cell motility via Girdin/APE. Dev Cell. 2005;9:389–402.
36 Morales M, Colicos MA, Goda Y. Actin-dependent regulation of neurotransmitter release at central synapses. Neuron. 2000;27: 539–550.
37 Shiojima I, Walsh K. Role of Akt signaling in vascular homeostasis and angiogenesis. Circ Res. 2002;90:1243–1250.

Decreased Myocardial β-Adrenergic Receptor Density in Relation to Increased Sympathetic Tone in Patients with Nonischemic Cardiomyopathy

Takahiro Tsukamoto[1], Koichi Morita[2], Masanao Naya[1], Masayuki Inubushi[2], Chietsugu Katoh[2], Kenichi Nishijima[3], Yuji Kuge[2], Hiroshi Okamoto[1], Hiroyuki Tsutsui[1], and Nagara Tamaki[2]

[1]Department of Cardiovascular Medicine, Hokkaido University Graduate School of Medicine, Sapporo, Japan; [2]Department of Nuclear Medicine, Hokkaido University Graduate School of Medicine, Sapporo, Japan; and [3]Faculty of Radiopharmaceutical Science, Health Sciences University of Hokkaido, Sapporo, Japan

Cardiac sympathetic function plays an important role in the regulation of left ventricular (LV) function and the pathophysiology of LV dysfunction. ^{11}C-CGP-12177 (^{11}C-CGP) has been used to assess myocardial β-adrenergic receptor (β-AR) density in vivo using PET. The aim of this study is to measure myocardial β-AR density in patients with nonischemic cardiomyopathy and to compare the measurements with various standard parameters of heart failure (HF), particularly with presynaptic function assessed by ^{123}I- metaiodobenzylguanidine (^{123}I-MIBG) imaging. **Methods:** ^{11}C-CGP PET was performed on 16 patients with nonischemic cardiomyopathy and 8 age-matched healthy volunteers using a double injection method. A ^{11}C-CGP dynamic scan for 75 min was performed after the injection of ^{11}C-CGP with a high specific activity. After 30 min, ^{11}C-CGP with a low specific activity was injected. The β-AR density of the whole LV was calculated on the basis of the graphical analysis method. Additionally, β-AR density was compared with LV ejection fraction (LVEF), sympathetic presynaptic function assessed using ^{123}I-MIBG kinetics, and neurohormonal parameters. **Results:** The β-AR density of patients was significantly lower than that of healthy volunteers (3.80 ± 0.96 vs. 7.70 ± 1.92 pmol/mL; $P < 0.0001$). In the patients, β-AR density correlated significantly with LVEF ($r = 0.62$, $P < 0.05$). Furthermore, β-AR density correlated significantly with the ^{123}I-MIBG washout rate ($r = -0.68$, $P < 0.01$) and delayed heart-to-mediastinum ratio (H/M ratio) ($r = 0.61$, $P < 0.05$). On the other hand, the correlation between β-AR density and early H/M ratio was not significant ($r = 0.40$, $P = 0.13$). The β-AR density of patients with severe HF (New York Heart Association functional [NYHA] class III) was significantly lower than that of those with NYHA functional class I or class II HF (3.24 ± 0.96 vs. 4.24 ± 0.73 pmol/mL; $P < 0.05$). **Conclusion:** A reduction in β-AR density measured by ^{11}C-CGP PET was observed in patients with nonischemic cardiomyopathy. This downregulation may be due to the increased presynaptic sympathetic tone as assessed by ^{123}I-MIBG imaging.

Key Words: β-adrenergic receptor; heart failure; sympathetic tone; norepinephrine

J Nucl Med 2007; 48:1777–1782
DOI: 10.2967/jnumed.107.043794

Heart failure (HF) is a major cause of mortality and represents a growing health problem, despite major therapeutic advances (*1–3*). The severity of HF is evaluated primarily by symptoms, clinical findings, hemodynamic measurements, left ventricular ejection fraction (LVEF), or exercise tolerance (*4–7*). In addition, the assessment of neurohormonal system disorders related to HF has proven to be valuable for risk stratification (*8–11*). Despite these indices, the accurate evaluation of the risk of mortality remains difficult.

Cardiac sympathetic function plays an important role in the regulation of heart function and has been studied extensively in recent decades (*12,13*). In a failing heart, the myocardial responsiveness to β-agonist stimulation is suppressed, primarily because of the downregulation of β1-adrenergic receptor (AR) (*14,15*). This β-AR downregulation has been induced by an enhanced sympathetic activity to the heart and an enhanced release of endogenous cardiac-derived catecholamines (*16*). The degree of downregulation is related to the severity of HF (*15*). Furthermore, these patients have higher levels of circulating catecholamines, which are inversely related to prognosis (*8*). On the basis of these findings, a beneficial effect of β-adrenergic blocker therapy has been hypothesized. In fact, many trials have shown the beneficial effect of β-blocker therapy in heart failure patients (*3*).

However, this in vitro measurement is invasive and does not allow longitudinal and regional assessment in humans. PET is an excellent noninvasive tool for investigating the distribution of myocardial β-AR in vivo and provides the

Received May 30, 2007; revision accepted Aug. 18, 2007.
For correspondence or reprints contact: Nagara Tamaki, MD, Department of Nuclear Medicine, Graduate School of Medicine, Hokkaido University, Kita15 Nishi7, Kita-ku, Sapporo 060-8638, Japan.
E-mail: natamaki@med.hokudai.ac.jp
COPYRIGHT © 2007 by the Society of Nuclear Medicine, Inc.

possibility of repeated measurements. Studies using PET and the radioligand ^{11}C-CGP-12177 (^{11}C-CGP) have shown promising results that are in agreement with those of in vitro studies (*17*). CGP appears to be the most suitable ligand because it is very potent and is a hydrophilic nonselective β-AR antagonist with low nonspecific binding on membranes and slight cellular uptake (*18*). CGP enables the investigation of plasma membrane receptors. However, CGP has not been studied extensively in vivo because of difficulty in the synthesis of ^{11}C-CGP. We developed a method for producing ^{11}C-CGP with very high yield and specific activity, which provides high-quality images and the clinical application for myocardial β-AR density (*19,20*).

Merlet et al. demonstrated the downregulation of β-AR in patients with HF caused by idiopathic dilated cardiomyopathy (*17*). We hypothesized that this downregulation may be related to the adrenergic presynaptic dysfunction. However, there is little information about the relationship between presynaptic function and β-AR density in HF. The aim of this study was to measure myocardial β-AR density in patients with nonischemic left ventricular (LV) dysfunction using ^{11}C-CGP PET and to compare the measured values with various standard parameters of HF and presynaptic function. Adrenergic presynaptic function was assessed by ^{123}I-metaiodobenzylguanidine (^{123}I-MIBG) imaging. ^{123}I-MIBG, a norepinephrine (NE) analog, is accumulated in sympathetic nerve endings through the uptake-1 mechanism and can be used to delineate cardiac sympathetic nerve distribution and function (*21–23*).

MATERIALS AND METHODS

Study Patients

In this study, we enrolled 16 patients diagnosed as having nonischemic cardiomyopathy (8 men, 8 women; mean age ± SD, 62.8 ± 11.1 y). All patients had LV dysfunction (LVEF < 45%) but showed normal coronary angiography. All patients underwent ^{11}C-CGP PET and ^{123}I-MIBG imaging within 1 mo (mean time, 15 d) during the stable stage of HF. No clinical events or changes in medication occurred during these 2 studies. Because treatment with a β-blocker is known to affect myocardial β-AR density, patients with a history of β-blocker treatment were excluded from the study.

Control Subjects

Eight age-matched healthy volunteers (6 men, 2 women; mean age ± SD, 57.6 ± 13.0 y; P = not significant vs. patients) served as control subjects for the measurements of β-AR density. They showed no sign of cardiac disease and each had a normal resting electrocardiogram. This study was approved by the Ethics Committee of Hokkaido University Hospital. All subjects gave their written informed consent for the study.

PET Data Acquisition

All PET scans were obtained using an ECAT EXACT HR+ (Siemens Medical Solutions, Inc.). A transmission scan was performed to correct photon attenuation for 8 min with a ^{68}Ge source. ^{11}C-CGP was prepared as reported previously (*21,22*). The measurement of myocardial β-AR density using ^{11}C-CGP PET was performed according to a modified double-injection protocol reported previously (*24,25*). During a 75-min dynamic emission scan, the first dose of ^{11}C-CGP with a high specific activity (169 ± 65 MBq, 0.19 ± 0.13 μg) was infused intravenously over a 2-min period. Thirty minutes later, the second dose of ^{11}C-CGP with a low specific activity (312 ± 145 MBq, 22.0 ± 1.8 μg) was again infused over a 2-min period. A 54-frame dynamic emission scan was used for measurement of the sequential distributions of the tracer in vivo. During the 30-min period after the start of the first infusion, 24 time frames (8 × 15-s, 4 × 30-s, 2 × 60-s, 2 × 120-s, and 8 × 150-s frames) were acquired. After the second infusion, the scan was completed with 30 frames (8 × 15-s, 4 × 30-s, 2 × 60-s, 2 × 120-s, and 14 × 150-s frames).

PET Data Analysis

All emission sinograms were reconstructed with filtered backprojection using a Hann filter (cutoff frequency, 0.3 cycle/pixel). The in-plane resolution was 4.5-mm full width at half maximum in the images reconstructed into a 128 × 128 matrix. All data were corrected for dead time, decay, and measured photon attenuation. A whole-heart region of interest (ROI) was set manually in each transaxial view. Myocardial time–activity curves in the ROIs were corrected for radioactive decay and for vascular activity using the regional values of blood volume. The sections of the curve corresponding to the 2 slow clearance phases, which represent the dissociation of ^{11}C-CGP bound to β-AR, were extrapolated back to the start of the infusions. β-AR density was then determined as the maximum number of available specific ^{11}C-CGP–binding sites per gram of tissue (B_{max}) in the ROIs using a modified equation described by Delforge et al. (*24,25*).

^{123}I-MIBG Data Acquisition and Analysis

^{123}I-MIBG (111 MBq) (Dai-ichi Radioisotope Laboratories, LTD.) was injected intravenously into the patients under resting and fasting conditions. Fifteen minutes and 4 h after the injection, static planar images were acquired in the anterior view using a dual-head γ-camera (ADAC Vertex Plus; Phillips) equipped with low-energy, general-purpose collimators. Static images on 512 × 512 matrices were collected for 5 min with a 20% window centered at 159 keV. Subsequently, SPECT of the heart was performed in 64 × 64 matrices using a filtered backprojection method for reconstruction. A ramp filter and a Butterworth filter with an order of 5.0 and a cutoff frequency of 0.50 cycle per pixel were used for reconstruction. No attenuation or scatter correction was performed. LV uptake was assessed by quantitative analysis performed manually drawing the ROI over the LV in the anterior view. The rectangular ROIs of 9 × 9 pixels were placed over the upper mediastinum. Counts per pixel were calculated from each ROI located in the heart and the mediastinum. The heart-to-mediastinum count ratios (H/M ratios) of early and delayed planar images were computed to quantify the cardiac uptake of ^{123}I-MIBG. The washout rate (WR) was calculated using the following formula:

$$\text{WR}\,(\%) = (\text{H at 15 min} - \text{H at 4 h})/(\text{H at 15 min} \times 100),$$

where H = mean counts per pixel in the LV.

Echocardiography

Echocardiography was performed in all patients at about the same time as ^{11}C-CGP PET. LVEF was measured from apical 2-chamber

and 4-chamber images using the biplane disk-summation method based on the standards of the American Society of Echocardiography (*26*).

Measurement of Neurohormonal Parameters

Before the PET study was started, venous blood samples were drawn after a 20-min resting period in the supine position. Plasma NE levels were measured using high-performance liquid chromatography. Plasma brain natriuretic peptide (BNP) levels were measured by chemiluminescent enzyme immunoassay.

Statistical Analysis

All data were expressed as mean ± SD. Regression analysis was performed using a linear regression method. A Student *t* test was performed to test differences between patients and control subjects. A *P* value < 0.05 was considered statistically significant. In addition, multivariate stepwise regression analyses were performed to investigate whether the β-AR density was associated independently with LVEF or NYHA class or whether it was dependent on presynaptic changes of plasma neurohumoral levels.

RESULTS

^{11}C-CGP was produced with a very high yield (1,964 ± 1,105 MBq) and specific activity (485 ± 370 GBq/μmol). The characteristics of the patients are shown in Table 1. Four patients were classified as New York Heart Association (NYHA) functional class I, 5 patients as class II, and 7 patients as class III at the time of the PET scan. Although the BNP levels of the patients were significantly higher than those of the control subjects (183 ± 143 vs. 26 ± 24 pg/mL; $P < 0.05$), there was no significant difference in the NE levels between the 2 groups (367 ± 235 vs. 249 ± 116 pg/mL; $P = 0.20$).

The calculated β-AR densities are shown in Figure 1. The β-AR density of the patients was significantly reduced by 51% in comparison with that of the control subjects (3.80 ± 0.96 vs. 7.70 ± 1.92 pmol/mL; $P < 0.0001$). In the patients, β-AR density correlated significantly with LVEF ($r = 0.62$, $P < 0.05$; Fig. 2). Furthermore, β-AR density showed good correlations with ^{123}I-MIBG WR ($r = -0.68$, $P < 0.01$; Fig. 3A) and delayed H/M ratio ($r = 0.61$, $P < 0.05$; Fig. 3B). The correlation between β-AR density and early H/M ratio was not significant ($r = 0.40$, $P = 0.13$; Fig. 3C). β-AR density showed no correlation with BNP levels ($r = -0.26$, $P = 0.33$) or NE levels ($r = -0.44$, $P = 0.09$).

β-AR density of the patients with severe HF (NYHA class III) was significantly lower than that of those with mild HF (NYHA class I or II) (3.24 ± 0.96 vs. 4.24 ± 0.73 pmol/mL, $P < 0.05$; Table 2). There were no significant differences in early H/M ratios (1.76 ± 0.41 vs. 2.01 ± 0.35; $P = 0.22$) and delayed H/M ratios (1.49 ± 0.40 vs. 1.88 ± 0.38; $P = 0.07$), WR (41.4% ± 6.1% vs. 37.2% ± 7.7%; $P = 0.26$), and BNP levels (201 ± 129 vs. 169 ± 159 pg/mL; $P = 0.66$) between these 2 groups. The LVEF (24.6% ± 11.0% vs. 36.0% ± 5.9%; $P < 0.05$) and NE levels (584 ± 188 vs. 198 ± 60 pg/mL; $P < 0.0001$) of the severe HF group were significantly lower than those of the mild HF group (Table 2).

β-AR density significantly correlated with NYHA class ($r = -0.61$, $P < 0.05$), LVEF, ^{123}I-MIBG WR, and delayed

TABLE 1
Clinical Characteristics of 16 Patients

Characteristic	Value
Age (y)	62.8 ± 11.1
Sex (M/F)	8/8
LVEF (%)	31.0 ± 10.1
BNP level (pg/mL)	183 ± 143
NE level (pg/mL)	367 ± 235
NYHA class*	
I	4 (25)
II	5 (31)
III	7 (44)
Medication*	
ACEI or ARB	14 (88)
Diuretics	12 (75)
Spironolactone	7 (44)
Digitalis	5 (31)

*Values are expressed as no. (%).
NYHA = New York Heart Association; ACEI = angiotensin-converting enzyme inhibitor; ARB = angiotensin II receptor blocker.

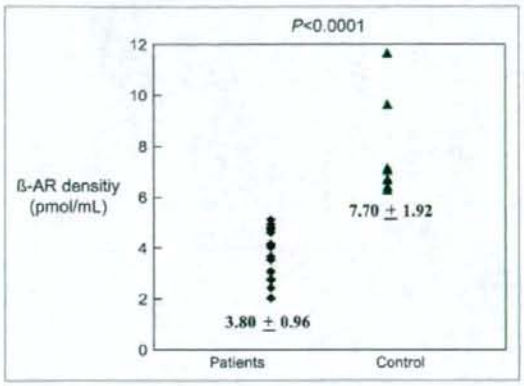

FIGURE 1. Comparison of β-AR density between patients with HF and control subjects.

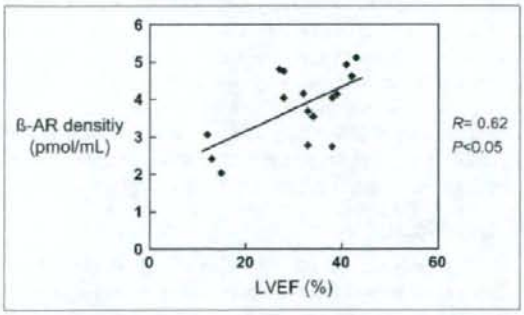

FIGURE 2. Relationship between LVEF and β-AR density.

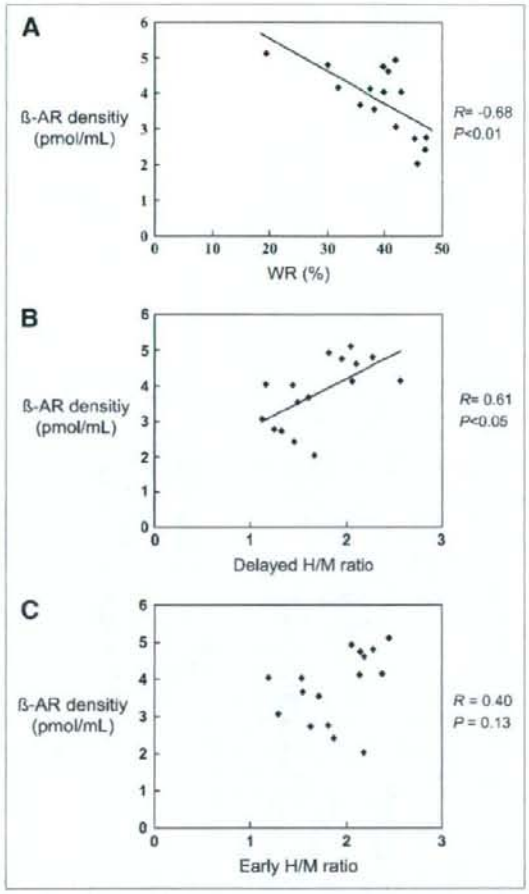

FIGURE 3. (A) Relationship between ^{123}I-MIBG WR and β-AR density. (B) Relationship between delayed ^{123}I-MIBG H/M ratio and β-AR density. (C) Relationship between early ^{123}I-MIBG H/M ratio and β-AR density.

H/M ratio. In multivariate analysis, delayed H/M ratio was excluded, because there was a significant correlation between ^{123}I-MIBG WR and delayed H/M ratio ($r = -0.62$, $P < 0.05$). ^{123}I-MIBG WR ($r = -0.70$) and NYHA class ($r = -0.50$) were the determinants of myocardial β-AR density by multivariate stepwise analysis. By multivariate stepwise analysis, β-AR density was the only significant determinant of LVEF ($r = 0.58$) among β-AR density, ^{123}I-MIBG WR, BNP level, and NE level. In contrast, NE level was the only determinant of NYHA class ($r = 0.73$).

DISCUSSION

This study showed that the myocardial β-AR density of the patients with nonischemic cardiomyopathy was significantly reduced by 51% in comparison with that of the age-matched control subjects. Myocardial β-AR density showed good correlations with LVEF, ^{123}I-MIBG WR, and delayed H/M ratio but not with plasma BNP level or NE level.

TABLE 2
NYHA Classification and Parameters of HF

Parameter	Mild HF (n = 9): NYHA class I or II	Severe HF (n = 7): NYHA class III	P value
β-AR density (pmol/mL)	4.24 ± 0.73	3.24 ± 0.96	<0.05
Early H/M ratio	2.01 ± 0.35	1.76 ± 0.41	0.22
Delayed H/M ratio	1.88 ± 0.38	1.49 ± 0.40	0.07
^{123}I-MIBG WR (%)	37.2 ± 7.7	41.4 ± 6.1	0.26
LVEF (%)	36.0 ± 5.9	24.6 ± 11.0	<0.05
BNP level (pg/mL)	169 ± 159	201 ± 129	0.66
NE level (pg/mL)	198 ± 60	584 ± 188	<0.0001

β-AR density was reduced with decreasing LVEF. Severe HF patients showed a greater reduction in β-AR density than mild HF patients, indicating that a decrease in β-AR density reflects the severity of HF. On the other hand, β-AR density showed no correlation with plasma BNP level or NE level. These neurohormonal levels may change rapidly depending on the condition of HF. Because this study was performed at the stable stage of HF, these neurohormonal levels might have already returned to near-normal levels. In contrast, it is not clear whether β-AR density may change so rapidly. Therefore, such chronological differences might possibly cause little or no significant correlation between β-AR density and these neurohormonal parameters.

Bristow et al. showed a reduction in β-AR density in a failing human heart using an in vitro ligand-binding technique (*14*). They reported 50%–56% reductions in β-AR density. In 1993 Merlet et al. reported in vivo measurements of β-AR density using PET and ^{11}C-CGP (*17*). They showed downregulation of β-AR by 53% with correlation with LVEF in the patients with idiopathic dilated cardiomyopathy. Our current results are in agreement with these previous reports.

Increased presynaptic activity in the failing human heart (*8,16*) and a decrease of postsynaptic β-AR density in failing heart (*14,15,17*) have been reported. In our study, the degree of β-AR downregulation corresponded to the increase in ^{123}I-MIBG WR and a decrease in delayed H/M ratio. Because MIBG is a NE analog, WR and delayed H/M ratio may directly reflect NE release from the nerve terminal and its reuptake into the nerve terminal (uptake-1). In addition, the ^{123}I-MIBG WR may reflect presynaptic sympathetic tone. The local NE concentration in the synaptic cleft increases when WR increases or delayed H/M ratio decreases (*21–23*). Our results may confirm the hypothesis that the increase in NE concentration in the synaptic cleft contributes to myocardial β-AR downregulation (*27–29*). Furthermore, the present study confirms pathophysiologic conditions of failing heart, which have been proven clinically over decades.

On the other hand, the correlation between β-AR density and early H/M ratio was not significant. It has been reported that an early MIBG uptake reflects only the integrity of presynaptic nerve terminals and their uptake-1 function, whereas a delayed MIBG uptake represents overall information with regard to neural function at the nerve terminal (*30*).

Schafers et al. reported β-AR downregulation and an impaired uptake-1 mechanism in patients with hypertrophic cardiomyopathy using ^{11}C-CGP and ^{11}C-hydroxyephedrin (^{11}C-HED) PET (*28*). In their study, all patients had preserved LV systolic function and no evidence of HF. To our knowledge, there is no information with regard to the relationship between presynaptic and postsynaptic functions in HF in vivo. Our results show a precise correlation between β-AR density estimated by ^{11}C-CGP PET and presynaptic function determined by ^{123}I-MIBG imaging in HF patients.

^{123}I-MIBG imaging has been widely used for the assessment of cardiac sympathetic function in HF (*22,23,31–34*). In many studies, it has been reported that impaired cardiac adrenergic innervation as assessed by ^{123}I-MIBG imaging was closely associated with mortality in patients with HF (*35–37*). Some studies demonstrated that ^{123}I-MIBG imaging was a good predictor of response to adrenergic β-blocker therapy (*38,39*). Spyrou et al. reported that β-AR downregulation can be used as a predictor of LV remodeling in patients after acute myocardial infarction (*40*). Further studies may be needed to evaluate the relationship between β-AR density, prognosis, and response to therapy in a larger patient population.

As a first limitation of this study, we used different methods for assessment of presynaptic and postsynaptic function. ^{11}C-HED enables quantitative assessment of presynaptic function using PET. Because presynaptic function was assessed using ^{123}I-MIBG imaging instead of ^{11}C-HED, an accurate quantification of presynaptic function might be limited. The resolution of ^{123}I-MIBG imaging is inferior to PET. Attenuation and scatter correction were not performed in this study. Myocardial ^{123}I-MIBG imaging was analyzed semiquantitatively by using the H/M ratio on early and delayed planar images and the myocardial WR. However, we do not believe that attenuation and scatter may affect these parameters, because these parameters were relative values calculated from the counts in the anterior planar images. On the other hand, MIBG has advantages for estimating the integrity of presynaptic nerve terminals, their uptake-1 function, and sympathetic tone. Although we applied commonly used parameters from MIBG imaging, a better quantitative measurement may be needed for further analysis.

Because the number of patients in this study was small ($n = 16$) and the follow-up time was limited, cardiac events were not observed in the patients. Thus, we did not evaluate the prognostic value of β-AR density in this study. However, because this parameter was correlated with LVEF, NYHA, and MIBG parameters, β-AR may have the potential for risk stratification in patients with HF. Further study is warranted to confirm the prognostic value.

CONCLUSION

Decreased cardiac β-AR density measured by ^{11}C-CGP PET was observed in patients with nonischemic cardiomyopathy. In addition, β-AR density correlated with ^{123}I-MIBG WR and delayed H/M ratio. This downregulation may be due to an accelerated presynaptic sympathetic tone.

REFERENCES

1. Studies of left ventricular dysfunction (SOLVD): rationale, design and methods—two trials that evaluate the effect of enalapril in patients with reduced ejection fraction. *Am J Cardiol.* 1990;66:315–322.
2. Pfeffer MA, Braunwald E, Moye LA, et al. Effect of captopril on mortality and morbidity in patients with left ventricular dysfunction after myocardial infarction: results of the survival and ventricular enlargement trial—the SAVE Investigators. *N Engl J Med.* 1992;327:669–677.
3. Packer M, Bristow MR, Cohn JN, et al. The effect of carvedilol on morbidity and mortality in patients with chronic heart failure: U.S. Carvedilol Heart Failure Study Group. *N Engl J Med.* 1996;334:1349–1355.
4. Schwarz F, Mall G, Zebe H, et al. Determinants of survival in patients with congestive cardiomyopathy: quantitative morphologic findings and left ventricular hemodynamics. *Circulation.* 1984;70:923–928.
5. Corbett JR, Dehmer GJ, Lewis SE, et al. The prognostic value of submaximal exercise testing with radionuclide ventriculography before hospital discharge in patients with recent myocardial infarction. *Circulation.* 1981;64:535–544.
6. Cintron G, Johnson G, Francis G, Cobb F, Cohn JN. Prognostic significance of serial changes in left ventricular ejection fraction in patients with congestive heart failure: the V-HeFT VA Cooperative Studies Group. *Circulation.* 1993; 87(suppl):VI17–VI23.
7. Mancini DM, Eisen H, Kussmaul W, Mull R, Edmunds LH Jr, Wilson JR. Value of peak exercise oxygen consumption for optimal timing of cardiac transplantation in ambulatory patients with heart failure. *Circulation.* 1991;83:778–786.
8. Cohn JN, Levine TB, Olivari MT, et al. Plasma norepinephrine as a guide to prognosis in patients with chronic congestive heart failure. *N Engl J Med.* 1984; 311:819–823.
9. Hall C, Rouleau JL, Moye L, et al. N-terminal proatrial natriuretic factor: an independent predictor of long-term prognosis after myocardial infarction. *Circulation.* 1994;89:1934–1942.
10. Omland T, Aakvaag A, Bonarjee VV, et al. Plasma brain natriuretic peptide as an indicator of left ventricular systolic function and long-term survival after acute myocardial infarction: comparison with plasma atrial natriuretic peptide and N-terminal proatrial natriuretic peptide. *Circulation.* 1996;93:1963–1969.
11. Tsutamoto T, Wada A, Maeda K, et al. Attenuation of compensation of endogenous cardiac natriuretic peptide system in chronic heart failure: prognostic role of plasma brain natriuretic peptide concentration in patients with chronic symptomatic left ventricular dysfunction. *Circulation.* 1997;96:509–516.
12. Bristow MR, Hershberger RE, Port JD, et al. Beta-adrenergic pathways in nonfailing and failing human ventricular myocardium. *Circulation.* 1990;82(suppl): I12–125.
13. Port JD, Bristow MR. Altered beta-adrenergic receptor gene regulation and signaling in chronic heart failure. *J Mol Cell Cardiol.* 2001;33:887–905.
14. Bristow MR, Ginsburg R, Minobe W, et al. Decreased catecholamine sensitivity and beta-adrenergic-receptor density in failing human hearts. *N Engl J Med.* 1982; 307:205–211.
15. Fowler MB, Laser JA, Hopkins GL, Minobe W, Bristow MR. Assessment of the beta-adrenergic receptor pathway in the intact failing human heart: progressive receptor down-regulation and subsensitivity to agonist response. *Circulation.* 1986; 74:1290–1302.
16. Ruffolo RR Jr, Kopia GA. Importance of receptor regulation in the pathophysiology and therapy of congestive heart failure. *Am J Med.* 1986;80:67–72.
17. Merlet P, Delforge J, Syrota A, et al. Positron emission tomography with ^{11}C CGP-12177 to assess beta-adrenergic receptor concentration in idiopathic dilated cardiomyopathy. *Circulation.* 1993;87:1169–1178.
18. Staehelin M, Simons P, Jaeggi K, Wigger N. CGP-12177: a hydrophilic beta-adrenergic receptor radioligand reveals high affinity binding of agonists to intact cells. *J Biol Chem.* 1983;258:3496–3502.

19. Nishijima K, Kuge Y, Seki K, et al. A simplified and improved synthesis of [^{11}C]phosgene with iron and iron (III) oxide. *Nucl Med Biol.* 2002;29:345–350.
20. Nishijima K, Kuge Y, Seki K, et al. Preparation and pharmaceutical evaluation for clinical application of high specific activity S-(-)-[^{11}C]CGP-12177, a radioligand for beta-adrenoreceptors. *Nucl Med Commun.* 2004;25:845–849.
21. Wieland DM, Brown LE, Rogers WL, et al. Myocardial imaging with a radioiodinated norepinephrine storage analog. *J Nucl Med.* 1981;22:22–31.
22. Henderson EB, Kahn JK, Corbett JR, et al. Abnormal I-123 metaiodobenzylguanidine myocardial washout and distribution may reflect myocardial adrenergic derangement in patients with congestive cardiomyopathy. *Circulation.* 1988; 78:1192–1199.
23. Schofer J, Spielmann R, Schuchert A, Weber K, Schluter M. Iodine-123 metaiodobenzylguanidine scintigraphy: a noninvasive method to demonstrate myocardial adrenergic nervous system disintegrity in patients with idiopathic dilated cardiomyopathy. *J Am Coll Cardiol.* 1988;12:1252–1258.
24. Delforge J, Syrota A, Lancon JP, et al. Cardiac beta-adrenergic receptor density measured in vivo using PET, CGP 12177, and a new graphical method. *J Nucl Med.* 1991;32:739–748.
25. Delforge J, Mesangeau D, Dolle F, et al. In vivo quantification and parametric images of the cardiac beta-adrenergic receptor density. *J Nucl Med.* 2002;43: 215–226.
26. Schiller NB, Shah PM, Crawford M, et al. Recommendations for quantitation of the left ventricle by two-dimensional echocardiography: American Society of Echocardiography Committee on Standards, Subcommittee on Quantitation of Two-Dimensional Echocardiograms. *J Am Soc Echocardiogr.* 1989;2:358–367.
27. Bristow MR, Minobe W, Rasmussen R, et al. Beta-adrenergic neuroeffector abnormalities in the failing human heart are produced by local rather than systemic mechanisms. *J Clin Invest.* 1992;89:803–815.
28. Schafers M, Dutka D, Rhodes CG, et al. Myocardial presynaptic and postsynaptic autonomic dysfunction in hypertrophic cardiomyopathy. *Circ Res.* 1998;82:57–62.
29. Mardon K, Montagne O, Elbaz N, et al. Uptake-1 carrier downregulates in parallel with the beta-adrenergic receptor desensitization in rat hearts chronically exposed to high levels of circulating norepinephrine: implications for cardiac neuroimaging in human cardiomyopathies. *J Nucl Med.* 2003;44:1459–1466.
30. Sisson JC, Wieland DM, Sherman P, Mangner TJ, Tobes MC, Jacques S Jr. Metaiodobenzylguanidine as an index of the adrenergic nervous system integrity and function. *J Nucl Med.* 1987;28:1620–1624.
31. Glowniak JV, Turner FE, Gray LL, Palac RT, Lagunas-Solar MC, Woodward WR. Iodine-123 metaiodobenzylguanidine imaging of the heart in idiopathic congestive cardiomyopathy and cardiac transplants. *J Nucl Med.* 1989;30:1182–1191.
32. Merlet P, Dubois-Rande JL, Adnot S, et al. Myocardial beta-adrenergic desensitization and neuronal norepinephrine uptake function in idiopathic dilated cardiomyopathy. *J Cardiovasc Pharmacol.* 1992;19:10–16.
33. Merlet P, Pouillart F, Dubois-Rande JL, et al. Sympathetic nerve alterations assessed with ^{123}I-MIBG in the failing human heart. *J Nucl Med.* 1999;40:224–231.
34. Cohen-Solal A, Rouzet F, Berdeaux A, et al. Effects of carvedilol on myocardial sympathetic innervation in patients with chronic heart failure. *J Nucl Med.* 2005; 46:1796–1803.
35. Merlet P, Valette H, Dubois-Rande JL, et al. Prognostic value of cardiac metaiodobenzylguanidine imaging in patients with heart failure. *J Nucl Med.* 1992; 33:471–477.
36. Merlet P, Benvenuti C, Moyse D, et al. Prognostic value of MIBG imaging in idiopathic dilated cardiomyopathy. *J Nucl Med.* 1999;40:917–923.
37. Momose M, Kobayashi H, Iguchi N, et al. Comparison of parameters of ^{123}I-MIBG scintigraphy for predicting prognosis in patients with dilated cardiomyopathy. *Nucl Med Commun.* 1999;20:529–535.
38. Suwa M, Otake Y, Moriguchi A, et al. Iodine-123 metaiodobenzylguanidine myocardial scintigraphy for prediction of response to beta-blocker therapy in patients with dilated cardiomyopathy. *Am Heart J.* 1997;133:353–358.
39. Kakuchi H, Sasaki T, Ishida Y, Komamura K, Miyatake K. Clinical usefulness of ^{123}I meta-iodobenzylguanidine imaging in predicting the effectiveness of beta blockers for patients with idiopathic dilated cardiomyopathy before and soon after treatment. *Heart.* 1999;81:148–152.
40. Spyrou N, Rosen SD, Path-Ordoubadi F, et al. Myocardial beta-adrenoceptor density one month after acute myocardial infarction predicts left ventricular volumes at six months. *J Am Coll Cardiol.* 2002;40:1216–1224.

Evaluation of Effects of Polymorphism for Metabolic Enzymes on Pharmacokinetics of Carvedilol by Population Pharmacokinetic Analysis

Yoh TAKEKUMA,*[a] Toru TAKENAKA,[b] Masami KIYOKAWA,[b] Koujiro YAMAZAKI,[b] Hiroshi OKAMOTO,[c] Akira KITABATAKE,[c] Hiroyuki TSUTSUI,[c] and Mitsuru SUGAWARA[b]

[a] *Laboratory of Pharmcotherapeutic Information, Department of Biopharmaceutical Sciences and Pharmacy, Faculty of Pharmaceutical Sciences, Hokkaido University; Kita-12-jo, Nishi-6-chome, Kita-ku, Sapporo 060–0812, Japan:* [b] *Department of Pharmacy, Hokkaido University Hospital; and* [c] *Department of Cardiovascular Medicine, Hokkaido University Hospital; Kita-14-jo, Nishi-6-chome, Kita-ku, Sapporo 060–8648, Japan.*
Received August 23, 2006; accepted November 18, 2006

In our previous study it was observed that the frequencies of *UGT1A1*6*, *UGT2B7*3* and *CYP2D6*10* in patients who have a low level ability of glucuronidation were significantly higher than those in patients with a high level of ability of glucuronidation. The same tendency was found in the frequency of *CYP2D6*5*, though there was no significant difference. The purpose of this study was to evaluate the effects of the polymorphism on pharmacokinetics of carvedilol by population pharmacokinetic analysis. Population pharmacokinetic analysis was performed using 373 plasma concentrations from 41 patients with chronic heart failure or angina pectoris. A one compartment pharmacokinetic model with first-order absorption (for oral dosing) was used to describe the concentration-*versus*-time data for carvedilol. We examined the effects of various clinical and genetic covariables in the regression models for clearance and volume of distribution. The results suggested that the factors of interindividual variation for carvedilol clearance were creatinine clearance and polymorphisms of *UGT2B7* and *CYP2D6* in the Japanese population with heart disease. It was estimated that *UGT2B7*3* decreased the clearance of carvedilol by 37%, but *UGT2B7*2* did not show any effect. Clearance in the patients who have intermediate activity of *CYP2D6* was decreased by 39%.

Key words CYP2D6; UDP-glucuronosyltransferase (UGT); population pharmacokinetics analysis; polymorphism; carvedilol

Carvedilol ((±)-1-carbazol-4-yloxy)-3-[[2-(*o*-methoxyphenoxy)ethyl]-amino]-2-propanol) is an anti-hypertensive and anti-anginal drug that has β-adrenergic blocking and vasodilating activities.[1,2] This drug has also recently been used to treat chronic heart failure (CHF). However, for treatment of CHF, it is recommended that the dose of carvedilol be gradually and carefully increased because of its negative inotropic activity.[2—5] Therefore, it is important to clarify factors that affect the pharmacokinetics of the drug.

Carvedilol is known to be metabolized into various metabolites by both oxidation and conjugation pathways in the liver. It is thought that the main pathway is direct glucuronidation of carvedilol because the main metabolite in plasma and urine was found to be the glucuronide of unchanged carvedilol (22% and 32%, respectively).[6,7] Three UDP-glucuronosyltransferase (UGT) isoforms have been reported to be capable of conjugating carvedilol into two forms of its glucuronide (G1 and G2).[8] UGT2B4 forms both glucuronides, whereas UGT1A1 (G2) and UGT2B7 (G1) forms either one. On the other hand, oxidation pathways are mainly catalyzed by CYP2D6.[9] CYP2D6 is responsible for the formation of 4′-hydroxy carvedilol and 5′-hydroxy carvedilol, and both metabolites are excreted into urine (6.4%).[7] Therefore, it is thought that the pharmacokinetics of carvedilol is complicated and that there are many factors in interindividual and intraindividual variation of its disposition.

We have reported that the frequencies of *UGT1A1*6*, *UGT2B7*3* and *CYP2D6*10* in patients who have a low level of ability of glucuronidation were significantly higher than those in patients with a high level of ability of glucuronidation. The same tendency was found in the frequency of *CYP2D6*5*, though there was no significant difference.[10] On the other hand, Honda *et al.* have reported that *CYP2D6*10* affected oral clearance of carvedilol but that *CYP2C9*3*, *CYP2C19*2*, *CYP2C19*3*, *CYP3A5*3*, *UGT2B7*2*, and *MDR1* C3435T did not significantly affect the pharmacokinetics of this drug in Japanese subjects.[11]

The aim of this study was to determine the effects of polymorphisms in *UGTs* and *CYP2D6* on pharmacokinetics of carvedilol using population pharmacokinetic analysis.

MATERIALS AND METHODS

The study protocol was approved by the Ethics Committee of the Graduate School of Medicine, Hokkaido University. Written informed consent for participation in the study was obtained from all subjects.

Patient Data The study population consisted of 41 patients (33 males and 8 females) with CHF or angina pectoris who were being treated with carvedilol. Data on plasma concentrations of carvedilol and its glucuronides, and that on their polymorphism for metabolic enzymes reported in our previous report with an additional subject were used.[10] The patients with CHF were classified into New York Heart Association (NYHA) classes II-III. The daily doses of carvedilol administered to the patients ranged from 1.25 to 40 mg, and the drug was taken in one or two doses daily. The age of patients was between 26 and 83 years (median age, 67 years), body weight (BW) varied between 32.3 and 98.9 kg (median BW, 61.9 kg). Their median creatinine clearance (Ccr) was 66.3 (15.9—131.1) ml/min, and no patients had clinically overt hepatic failure. There were no concomitantly used drugs that have been reported to strongly influence the plasma concentration of carvedilol.

Determination of Carvedilol and Its Alucuronide Plasma concentrations of carvedilol and its glucuronide were

* To whom correspondence should be addressed. e-mail: y-kuma@pharm.hokudai.ac.jp
© 2007 Pharmaceutical Society of Japan

determined by reversed-phase high-performance liquid chromatography (HPLC) with a fluorometric detector according to our previous report.[10] The separation was performed on a GL-Pak Nucleosil 100-5C8 4.6×250 mm I.D. column (GL Science Inc., Tokyo, Japan). The mobile phase was a mixture of acetonitrile and 50 mM potassium dihydrogenphosphate (28 : 72) containing a final concentration of 5 mM tetra-*n*-butylammonium chloride. The flow rate was 1.0 ml/min and column temperature was 40 °C. Excitation and emission wavelengths of 240 nm and 340 nm, respectively, were used for fluorometric detection. The sample preparation was done using the liquid layer extraction with diethyl ether. The determination of total concentration (carvedilol plus carvedilol glucuronide) was done after converting the glucuronide to parent carvedilol by β-glucuronidase. The concentration of the glucuronide was calculated by subtracting the concentration of the unchanged form from the total concentration.

Genotyping Genomic DNA was prepared using standard methods. The exons of *UGT1A1*, *UGT2B4* and *UGT2B7* genes (containing the promoter region of *UGT1A1*) in the 41 patients from whom written informed consent was obtained for genotyping were sequenced.[10] Each exon was amplified from genomic DNA (20—60 ng) using 0.5 units of Ex-*Taq* (Takara Bio Inc., Shiga, Japan) with 1 μM of the primers shown in our previous report.[10] The products were directly sequenced using a Big Dye Terminator Cycle Sequencing Kit (Applied Biosystems, Foster City, CA, U.S.A.) according to the manufacturer's recommended protocol.

For *CYP2D6* variants, the same 41 patients were genotyped. Mutant alleles that have been reported to have high frequencies in the Japanese population were selected in this study.[12] Genotyping of *CYP2D6*5* (deletion of the *CYP2D6* allele) was carried out using an amplification refractory mutation system (ARMS) assay as described by Johansson *et al.*[13] and Steen *et al.*[14] with minor modification. Genotyping of 100C>T (common SNP to *CYP2D6*4*, **10*, **14*, **36*, **37*, **47* and **49*) was carried out using the ARMS assay as described by Johansson *et al.*[15] Then samples that had the 100T allele were genotyped on *CYP2D6*4* and *CYP2D6*14*. Genotyping of *CYP2D6*4* and *CYP2D6*14* was carried out using the ARMS assay[16] and the PCR-restriction fragment length polymorphism (RFLP) assay.[17] In this study, subjects with 100C>T mutation were classified into *CYP2D6*10* except for *CYP2D6*4* and **14* because frequencies of *CYP2D6*18*, **21*, **36*, **37*, **47* and **49* are rare in the Japanese population.[12]

Population Pharmacokinetic Analysis Population pharmacokinetic modeling was performed using WinNonMix Professional (Version 2.0.1; Pharsight Corp., Mountain View, CA, U.S.A.) bundled with Compaq Visual Fortran (Standard Edition, Version 6.6; Compaq Computer Corp., Houston, TX, U.S.A.). A one compartment pharmacokinetic model with first-order absorption (for oral dosing) was used to describe the concentration-*versus*-time data for carvedilol. Pharmacokinetic parameters estimated were ka (first-order absorption rate constant), Vd/F (apparent volume of distribution), and CL/F (oral clearance).

The interpatient variability in CL/F was modeled as an exponential deviation from the 'true' parameter values (assuming a log normal distribution):

$$(CL/F)_i = (\overline{CL/F}) \cdot e^{\eta_i}$$

where $(CL/F)_i$ is the observed value of oral clearance in the ith individual, $\overline{CL/F}$ is the population parameter value predicted by the regression model, and η_i is random variable that is normally distributed with mean zero and variance ω^2 and represents the interpatient variability in the study population.

The residual error (intrapatient variability), which describes the difference between the observed and predicted concentrations, was modeled as a constant coefficient of variation:

$$C_{ij} = \overline{C_{ij}} \cdot (1+\varepsilon_{ij})$$

where C_{ij} is the jth observed concentration in the ith individual, $\overline{C_{ij}}$ is the jth predicted concentration in the ith individual, and ε_{ij} is the residual error, which is normally distributed with mean zero and variance σ^2, and represents the interpatient variability in the study population.

Once the base model had been defined, the effects of various clinical and genetic covariables in the regression models for clearance and volume of distribution were evaluated. Each covariable was added sequentially and then (when significant) cumulatively to the initial regression model. The effects of the following covariables on the population pharmacokinetics (PPK) model parameters were examined: body weight, Ccr, metabolic activity, and genotypes of *UGT1A1*, *UGT2B7* and *CYP2D6*. The effect of each covariable on the pharmacokinetic parameters was determined by forward univariable analysis. The effect on the objective function value (OFV) obtained before and after the addition of covariables is approximately χ^2 distributed with degrees of freedom equal to the number of parameters that are set to the null hypothesis values. A change in the OFV>7.88 ($p<0.005$) was accepted as statistically significant.

Model Validation To validate the model and the population pharmacokinetic parameter estimates, we used the bootstrap resampling technique.[18] The bootstrap method was used to evaluate the stability and confirm the robustness of the final model structured in this study. Two hundred bootstrap data sets were generated, and the same model was fitted to data for each of the 200 data sets. The average (mean), standard error (S.E.) and 95% confidence interval (95% C.I) for parameters from bootstrap data sets were calculated and compared with the original parameter estimates.

RESULTS AND DISCUSSION

Carvedilol is used clinically as a racemic mixture of *R*(+)- and *S*(−)-enantiomers.[19,20] The *S*(−) enantiomer is metabolized faster than the *R*(+) enantiomer. Only the *S*(−) enantiomer has β-adrenergic blocking activity, but both enantiomers have vasodilating activity based on α-blockade. It has been reported that carvedilol may be more effective for CHF patients than other beta-blockers such as metoprolol and bisoprolol because carvedilol has both β- and α- adrenergic blocking activities.[21] However, the magnitude of the effect on CHF of each enantiomer is unknown. Furthermore, control of dosage and determination of effects of carvedilol therapy have been done as a racemic mixture; therefore, we investigated the pharmacokinetics of carvedilol as a racemic

mixture in this study.

Population pharmacokinetic analysis was performed using 373 plasma concentrations from the 41 patients. The results of model building for pharmacokinetic parameters of carvedilol are shown in Table 1. Random variables of Vd/F and ka could not be estimated. Ccr and BW significantly reduced the OFV (>7.88). But BW was excluded from the model because the fixed effect value (θ_3) of BW was very low when Ccr and BW were added simultaneously. Ccr calculated by the Cockcroft–Gault equation may include the factor of BW. It is known that carvedilol is primarily eliminated by metabolism.[7] Therefore, our result was contradictory. Recently, it has been reported that decrease in Ccr is related to decrease in total clearance of a drug that is mainly eliminated by metabolism other than carvedilol. van Hest *et al.* reported that the pharmacokinetics of the immunosuppressant mycophenolic acid (MPA), which is mainly eliminated by metabolism (the ratio of excretion of the urinary unchanged drug amount being less than 1%), is affected by decrease in Ccr.[22] It is known that large amounts of UGTs are expressed in the kidney[23,24] and that intrinsic clearance (CL_{int}) of MPA in the kidney is greater than that in the liver.[25] It has been reported that the expression levels of some UGT isoforms were slightly decreased by inflammation and infection in mice.[26] However, it has not yet been directly proved that a decrease in Ccr is related to a decrease in activity of UGTs. Another possibility is that a decrease in glomerular filtration rate causes a decrease in metabolism in the process of reabsorption in uriniferous tubule epitheliocytes. In this study, it is thought that the effect of Ccr on CL/F reflected UGT activities.

Table 1. Summary of Model Building Step for Pharmacokinetic Parameters of Carvedilol

No.	Model equation	OFV	ΔOFV	Comparison	*p* value
1	$Vd/F=\theta_1$ $ka=\theta_2$ $CL/F=\theta_3 \cdot e^{\eta_1}$	1861.12	—	—	—
2	$Vd/F=\theta_1$ $ka=\theta_2$ $CL/F=\theta_3 \cdot BW \cdot e^{\eta_1}$	1839.96	21.16	*vs.* 1	$p<0.001$
3	$Vd/F=\theta_1$ $ka=\theta_2$ $CL/F=(\theta_3 \cdot BW+\theta_4 \cdot Ccr) \cdot e^{\eta_1}$	1679.96	160.00	*vs.* 2	$p<0.001$
4	$Vd/F=\theta_1$ $ka=\theta_2$ $CL/F=\theta_4 \cdot Ccr \cdot e^{\eta_1}$	1679.91	−0.05	*vs.* 3	N. S
5	$Vd/F=\theta_1 \cdot BW$ $ka=\theta_2$ $CL/F=\theta_4 \cdot Ccr \cdot e^{\eta_1}$	1681.08	−1.17	*vs.* 4	N. S

OFV: objective function value, ΔOFV: difference in OFV, BW: body weight (kg), Ccr: creatinine clearance (ml/min, observed or estimated value by Cockcroft–Gault equation), N.S: not significant. ΔOFV >7.88 ($p<0.005$) was accepted as statistically significant.

Metabolic activities of carvedilol were examined to improve the OFV. Table 2 shows the results of genotyping for *UGT1A1*, *UGT2B7* and *CYP2D6* that we reported previously together with the results for an additional subject.[10] We divided subjects into those with high and low level of ability of glucuronidation based on the ratio of glucuronide to unchanged carvedilol adjusted by Ccr, which affects clearance of glucuronide. Since clearance of carvedilol glucuronide depends on renal function, we defined the metabolic index (MI) as follows:

$$MI=(AUC_{glucuronized} \times Ccr)/AUC_{unchanged} \quad (1)$$

where $AUC_{glucuronized}$ and $AUC_{unchanged}$ are *AUC* of glucuronized carvedilol and *AUC* of unchanged carvedilol, respectively, and Ccr is creatinine clearance.

The effects of MI and polymorphism of metabolic en-

Table 2. Results of Genotyping in the 41 Patients

Low level of glucuronidation ability						High level of glucuronidation ability					
Subject	Ability of glucuronidation	*UGT1A1*	*UGT2B4*	*UGT2B7*	*CYP2D6*	Subject	Ability of glucuronidation	*UGT1A1*	*UGT2B4*	*UGT2B7*	*CYP2D6*
A	3.5	*1/*28	*1/*1	*2/*3	*1/*10	a	86.5	*1/*28	*1/*1	*1/*2	*1/*1
B	5.1	*1/*1	*1/*1	*1/*2	*10/*10	b	90.1	*1/*28	*1/*1	*1/*1	*1/*1
C	10.5	*1/*6	*1/*1	*1/*1	*5/*10	c	92.2	*1/*1	*1/*1	*1/*2	*1/*10
D	10.6	*1/*6	*1/*1	*1/*1	*10/*10	d	100.5	*1/*28	*1/*1	*1/*2	*1/*1
E	17.0	*1/*1	*1/*1	*1/*3	*1/*5	e	107.9	*1/*28	*1/*1	*1/*1	*1/*5
F	18.7	*1/*6	*1/*1	*1/*3	*1/*1	f	117.5	*1/*1	*1/*1	*2/*3	*1/*10
G	24.7	*1/*1	*1/*1	*1/*2	*10/*10	g	119.5	*6/*28	*1/*1	*1/*1	*1/*1
H	25.6	*1/*6	*1/*1	*1/*2	*10/*10	h	126.6	*1/*28	*1/*1	*1/*1	*1/*1
I	26.1	*1/*6	*1/*1	*3/*3	*1/*10	i	139.8	*1/*1	*1/*1	*1/*1	*4/*10
J	28.2	*6/*6	*1/*1	*1/*1	*1/*1	j	140.8	*1/*1	*1/*1	*2/*3	*1/*1
K	34.8	*1/*6	*1/*1	*2/*3	*1/*10	k	143.2	*1/*28	*1/*1	*2/*2	*1/*10
L	38.3	*1/*6	*1/*1	*1/*1	*1/*10	l	157.9	*1/*1	*1/*1	*1/*2	*1/*1
M	40.7	*1/*1	*1/*1	*1/*2	*1/*10	m	223.1	*1/*28	*1/*1	*1/*2	*1/*10
N	41.0	*1/*28	*1/*1	*1/*2	*1/*1	n	240.9	*1/*1	*1/*1	*2/*2	*1/*1
O	46.8	*1/*1	*1/*1	*2/*2	*1/*5	o	269.3	*1/*1	*1/*1	*2/*3	*1/*1
P	49.1	*1/*6	*1/*1	*1/*2	*1/*10	p	387.9	*1/*1	*1/*1	*1/*2	*1/*10
Q	56.0	*1/*1	*1/*1	*3/*3	*1/*1	q	504.4	*1/*1	*1/*1	*1/*2	*1/*10
R	65.1	*1/*6	*1/*1	*2/*3	*1/*10	r	1491.7	*1/*1	*1/*1	*1/*1	*1/*10
S	73.6	*1/*6	*1/*1	*1/*1	*1/*10						
T	77.5	*1/*28	*1/*1	*2/*3	*1/*10						
U	82.9	*1/*6	*1/*1	*1/*2	*10/*10						
V	84.0	*1/*6	*1/*1	*1/*1	*1/*10						
W	86.1	*1/*1	*1/*1	*3/*3	*1/*10						

Data from our previous report,[10] one additional patient.

Table 3. Effects of Metabolic Activity and Polymorphism for Metabolic Enzymes on CL/F of Carvedilol

No.	Model equation	OFV	ΔOFV	Comparison	p value
4	$CL/F=\theta_4\cdot Ccr\cdot e^{\eta_1}$	1679.91	—	—	—
6	$CL/F=\theta_4\cdot Ccr\cdot \theta_5^{MI}\cdot e^{\eta_1}$	1624.41	55.50	*vs.* 4	$p<0.001$
7	$CL/F=\theta_4\cdot Ccr\cdot \theta_6^{UGT1A1*6}\cdot e^{\eta_1}$	1678.05	1.86	*vs.* 4	N. S
8	$CL/F=\theta_4\cdot Ccr\cdot \theta_7^{UGT1A1*28}\cdot e^{\eta_1}$	1679.83	0.08	*vs.* 4	N. S
9	$CL/F=\theta_4\cdot Ccr\cdot \theta_8^{UGT2B7*2}\cdot e^{\eta_1}$	1677.46	2.45	*vs.* 4	N. S
10	$CL/F=\theta_4\cdot Ccr\cdot \theta_9^{UGT2B7*3m}\cdot e^{\eta_1}$	1667.43	12.48	*vs.* 4	$p<0.001$
11	$CL/F=\theta_4\cdot Ccr\cdot \theta_9^{UGT2B7*3m}\cdot \theta_{10}^{UGT2B7*3h}\cdot e^{\eta_1}$	1660.73	6.70	*vs.* 10	N. S
12	$CL/F=\theta_4\cdot Ccr\cdot \theta_{11}^{CYP2D6IM}\cdot e^{\eta_1}$	1663.08	16.83	*vs.* 4	$p<0.001$
13	$CL/F=\theta_4\cdot Ccr\cdot \theta_{12}^{CYP2D6*10m}\cdot e^{\eta_1}$	1655.51	7.57	*vs.* 12	N. S
14	$CL/F=\theta_4\cdot Ccr\cdot \theta_9^{UGT2B7*3m}\cdot \theta_{11}^{CYP2D6IM}\cdot e^{\eta_1}$	1623.48	43.95	*vs.* 10	$p<0.001$

OFV: objective function value, ΔOFV: difference in OFV, Ccr: creatinine clearance (ml/min, observed or estimated value by Cockcroft–Gault equation), MI: 1 for low level of glucuronidation ability and 0 for high level, UGT1A1*28, UGT1A1*6, UGT2B7*2 and UGT2B7*3m: 1 for hetero or homo type of each mutant allele and 0 for the other, UGT2B7*3h: 1 for homo type and 0 for the other, CYP2D6IM: 1 for intermediate metabolizer and 0 for extensive metabolizer, CYP2D6*10m: 1 for hetero type of each allele and 0 for the other, N.S: not significant. ΔOFV>7.88 ($p<0.005$) was accepted as statistically significant. Vd/F and ka was unchanged in this step.

zymes on the regression model are shown in Table 3. The OVF was improved most when MI was added to model. Therefore, MI was thought to be a good indicator of carvedilol clearance.

Among the polymorphisms for metabolic enzymes, those for *UGT2B7* and *CYP2D6* significantly decreased the OVF. In the *UGT2B4* gene, no missense SNP was found in our study.[10] On the other hand, polymorphisms of *UGT1A1* (*UGT1A1*6* and **28*) did not affect the model improvement, although the frequency of *UGT1A1*6* in the low level ability of glucuronidation group was significantly higher than that in the high level group in our previous study.[10] The reason is that the contribution of UGT1A1 to carvedilol metabolism is less than that of the other enzymes. The fact is that CL_{int} of UGT1A1 was lower than those of UGT2B4 and UGT2B7 in a previous report,[8] and that the difference of the allele frequencies between low and high ability of glucuronidation groups was observed in only *UGT1A1*6* but not *UGT1A6*28*, in spite of reduction of the enzyme activity in both mutation alleles in our previous study.[10] In UGT2B7, *UGT2B7*3* significantly decreased the OFV, but *UGT2B7*2* showed no effect. No remarkable functional difference between *UGT2B7*1* and *UGT2B7*2* alleles was found in several studies,[27—30] and our results are in agreement with the results of those studies. When the subjects with *UGT2B7*3* alleles were divided into heterozygous (*1/*3) and mutant-type homozygous, a tendency for OFV to decrease was observed, though there was no significant difference (Eq. 10 *versus* Eq. 11 in Table 3). Our results suggested that *UGT2B7*3* significantly decreased CL/F of carvedilol. *UGT2B7* polymorphism among the three UGT isoforms that are responsible for glucuronidation of carvedilol has a very important role in pharmacokinetics of carvedilol because the CL_{int} value of UGT2B7 is similar to that of UGT2B4 and is much greater than that of UGT1A1,[8] and UGT2B7 is expressed not only in the liver but also in the intestine.[24,31] Therefore, it is thought that only *UGT2B7*3* in UGTs affected the CL/F of carvedilol significantly and that polymorphism of UGT1A1 did not.

The patients were divided into extensive metabolizers (EM) and intermediate metabolizers (IM) based on genotyping of *CYP2D6*. IM included patients with *CYP2D6*1/*4*, **1/*5* and **10/*10*, because it has been shown that alleles of *CYP2D6*4* and **5* lack catalytic activity and that *CYP2D6*10* has partial activity.[13,32,33] On the other hand, EM included patients with the other genotypes observed in our study (*CYP2D6*1/*1* and **1/*10*). Poor metabolizers (*CYP2D6*5/*5*, **4/*4 etc.*) were not observed in this population. Polymorphism of *CYP2D6* significantly decreased the OVF. When the subjects with *CYP2D6*10* alleles were divided into heterozygous (**1/*10*) and mutant-type homozygous, a tendency for OFV to decrease was observed, though there was no significant difference (Eq. 12 *versus* Eq. 13 in Table 3). It has been shown using PPK analysis in healthy volunteers that *CYP2D6*10* decreased oral clearance of carvedilol[34]; therefore, our results are viewed as reasonable. A significant difference might be found for patients with heterozygous *UGT2B7*3* and patients with heterozygous *CYP2D6*10* if there were a larger number of subjects.

The final model consisted of Ccr, *UGT2B7* polymorphism and *CYP2D6* polymorphism as covariables for CL/F (Table 3, No. 12). Fixed effect values (θ_9, θ_{11}) of *UGT2B7* and *CYP2D6* polymorphisms are shown in Table 4. CL/F of the patients with *UGT2B7*3* was decreased by 37% and CL/F of the patients with IM of *CYP2D6* was also decreased by 39%. The results suggest that UGT2B7 and CYP2D6 are responsible for the metabolism of carvedilol and that polymorphisms of both enzymes have remarkable effect on the drug's clearance. This is the first study to demonstrate the contribution of

Table 4. Pharmacokinetic Parameters Estimated of Final Model for Carvedilol

Parameter	Estimated values	CV%
Vd/F (l)		
$Vd/F=\theta_1$		
θ_1	738.3	11.4
ka (h^{-1})		
$ka=\theta_2$	0.81	21.5
θ_2		
CL/F (l/h)		
$CL/F=\theta_4\cdot Ccr\cdot \theta_9^{UGT2B7*3m}\cdot \theta_{11}^{CYP2D6IM}$		
θ_4	0.89	8.2
θ_9: effect of *UGT2B7*3* allele	0.63	18.8
θ_{11}: effect of *CYP2D6*mutant allele	0.61	14.2
Interindividual variability (ω) in CL/F (%)	28.1	39.0
Intraindividual variability (σ: %)	71.1	13.2

UGT2B7*3: 1 for hetero or homo type of each mutant allele and 0 for the other, CYP2D6: 1 for intermediate metabolizer and 0 for extensive metabolizer.

Table 5. Population Pharmacokinetic Parameters Estimated by the Bootstrap Method

Parameter		Estimated value	Bootstrap		
			Mean	S.E.	95% C.I.
Vd/F (l)	θ_1	738.3	747.2	9.71	734—761
ka (h^{-1})	θ_2	0.81	0.90	0.28	0.850—0.959
CL/F (l/h)	θ_4	0.89	0.90	0.0050	0.886—0.906
	θ_9: effect of *UGT2B7*3* allele	0.63	0.63	0.0091	0.615—0.651
	θ_{11}: effect of *CYP2D6* mutant allele	0.61	0.63	0.0085	0.611—0.645

UGT2B7 mutation to carvedilol clearance *in vivo*, although there are some reports of the contribution of *CYP2D6* mutation to its clearance.[11,34,35] Our results indicated that the effect of *UGT2B7* mutation was as important for carvedilol pharmacokinetics as that of *CYP2D6*. However, estimated interindividual variability (σ) in this study was high (71.1%). Therefore, it is thought that there is another factor that affects the pharmacokinetics of carvedilol. It has been reported that carvedilol and its glucuronides are substrates of multiple-drug resistance protein 1 (*MDR1*) and MRP2[36,37] and that the *AUC* of carvedilol is related to these expression levels.[35] In our results, polymorphisms of metabolic enzymes are not sufficient to explain the individual differences in pharmacokinetics; therefore, it is possible that *MDR1* and MRP2 influence the bioavailability of carvedilol. However, the magnitudes of their effects are unknown. Giessmann *et al.* reported that rifampicin, which up-regulates both MDR1 and MRP2 but not CYP2D6, decreased the *AUC* of carvedilol independently of the *CYP2D6* genotype and increased the amount of fecal excretion after the drug's intravenous administration.[35] However, refampicin increases not only the expression levels of MDR1 and MRP2 but also those of UGTs.[38,39] Therefore, the reason for the increase in excretion in feces may be that increase in UGT in the liver caused an increase in metabolism and then the metabolites were excreted into bile *via* MDR1 or/and MRP2. Furthermore, Honda *et al.* reported that MDR1 C3435T did not significantly affect the pharmacokinetics of carvedilol in Japanese subjects.[11] In the study by Giessmann *et al.*, MDR1 protein level was not related to disposition of carvedilol.[35] When these findings are taken into consideration, it is still not clear which UGT, MDR1 or MRP2, has a greater effect on the pharmacokinetics of carvedilol.

The validation of this model and the population pharmacokinetic parameter estimates were carried out using the bootstrap method. Two hundred bootstrap data sets were generated, and the same model was fitted with each data set. The results of the validation are shown in Table 5. The mean values of the bootstrap estimtes for each PPK parameter were comparable with the original PPK parameter estimates. The value of parameter obtained from bootstrap data sets was almost the same as the value estimated from the original data set (each residue<11.1%). Furthermore, S.E. of each parameter from bootstrap data was very low. Therefore, there was no problem in the stability and the robustness of the final model structured in this study.

CONCLUSION

In conclusion, our results suggest that the factors responsible for interindividual variation in carvedilol clearance in the Japanese population with heart disease are Ccr and polymorphisms of *UGT2B7* and *CYP2D6*. It was estimated that *UGT2B7*3* decreased the clearance by 37%, but that *UGT2B7*2* had no effect, and IM of *CYP2D6* decreased the clearance by 39%.

REFERENCES

1) von Mollendorff E., Abshagen U., Akpan W., Neugebauer G., Schroter E., *Clin. Pharmacol. Ther.*, **39**, 677—682 (1986).
2) Frishman W. H., *N. Engl. J. Med.*, **339**, 1759—1765 (1998).
3) Packer M., Bristow M. R., Cohn J. N., Colucci W. S., Fowler M. B., Gilbert E. M., Shusterman N. H., *N. Engl. J. Med.*, **334**, 1349—1355 (1996).
4) Cice G., Ferrara L., D'Andrea A., D'Isa S., Di Benedetto A., Cittadini A., Russo P. E., Golino P., Calabro R., *J. Am. Coll. Cardiol.*, **41**, 1438—1444 (2003).
5) Keating G. M., Jarvis B., *Drugs*, **63**, 1697—1741 (2003).
6) Neugebauer G., Akpan W., von Mollendorff E., Neubert P., Reiff K., *J. Cardiovasc. Pharmacol.*, **10** (Suppl. 11), S85—S88 (1987).
7) Neugebauer G., Neubert P., *Eur. J. Drug Metab. Pharmacokinet.*, **16**, 257—260 (1991).
8) Ohno A., Saito Y., Hanioka N., Jinno H., Saeki M., Ando M., Ozawa S., Sawada J., *Drug Metab. Dispos.*, **32**, 235—239 (2004).
9) Oldham H. G., Clarke S. E., *Drug Metab. Dispos.*, **25**, 970—977 (1997).
10) Takekuma Y., Takenaka T., Kiyokawa M., Yamazaki K., Okamoto H., Kitabatake A., Tsutsui H., Sugawara M., *J. Pharm. Pharm. Sci.*, **9**, 101—112 (2006).
11) Honda M., Ogura Y., Toyoda W., Taguchi M., Nozawa T., Inoue H., Hashimoto Y., *Biol. Pharm. Bull.*, **29**, 772—778 (2006).
12) Soyama A., Kubo T., Miyajima A., Saito Y., Shiseki K., Komamura K., Ueno K., Kamakura S., Kitakaze M., Tomoike H., Ozawa S., Sawada J., *Drug Metab. Pharmacokinet.*, **19**, 313—319 (2004).
13) Johansson I., Oscarson M., Yue Q. Y., Bertilsson L., Sjoqvist F., Ingelman-Sundberg M., *Mol. Pharmacol.*, **46**, 452—459 (1994).
14) Steen V. M., Andreassen O. A., Daly A. K., Tefre T., Borresen A. L., Idle J. R., Gulbrandsen A. K., *Pharmacogenetics*, **5**, 215—223 (1995).
15) Johansson I., Lundqvist E., Dahl M. L., Ingelman-Sundberg M., *Pharmacogenetics*, **6**, 351—355 (1996).
16) Heim M., Meyer U. A., *Lancet.*, **336**, 529—532 (1990).
17) Wang S. L., Lai M. D., Huang J. D., *Drug Metab. Dispos.*, **27**, 385—388 (1999).
18) Ette E. I., *J. Clin. Pharmacol.*, **37**, 486—495 (1997).
19) Neugebauer G., Akpan W., Kaufmann B., Reiff K., *Eur. J. Clin. Pharmacol.*, **38** (Suppl. 2), S108—S111 (1990).
20) Morgan T., *Clin. Pharmacokinet.*, **26**, 335—346 (1994).
21) Poole-Wilson P. A., Swedberg K., Cleland J. G., Di Lenarda A., Hanrath P., Komajda M., Lubsen J., Lutiger B., Metra M., Remme W. J., Torp-Pedersen C., Scherhag A., Skene A., *Lancet*, **362**, 7—13 (2003).
22) van Hest R. M., van Gelder T., Vulto A. G., Mathot R. A., *Clin. Pharmacokinet.*, **44**, 1083—1096 (2005).
23) McGurk K. A., Brierley C. H., Burchell B., *Biochem. Pharmacol.*, **55**, 1005—1012 (1998).
24) Tukey R. H., Strassburg C. P., *Annu. Rev. Pharmacol. Toxicol.*, **40**, 581—616 (2000).
25) Bowalgaha K., Miners J. O., *Br. J. Clin. Pharmacol.*, **52**, 605—609 (2001).

26) Richardson T. A., Sherman M., Kalman D., Morgan E. T., *Drug Metab. Dispos.*, **34**, 351—353 (2006).
27) Bhasker C. R., McKinnon W., Stone A., Lo A. C., Kubota T., Ishizaki T., Miners J. O., *Pharmacogenetics*, **10**, 679—685 (2000).
28) Holthe M., Klepstad P., Zahlsen K., Borchgrevink P. C., Hagen L., Dale O., Kaasa S., Krokan H. E., Skorpen F., *Eur. J. Clin. Pharmacol.*, **58**, 353—356 (2002).
29) Holthe M., Rakvag T. N., Klepstad P., Idle J. R., Kaasa S., Krokan H. E., Skorpen F., *Pharmacogenomics J.*, **3**, 17—26 (2003).
30) Court M. H., Krishnaswamy S., Hao Q., Duan S. X., Patten C. J., von Moltke L. L., Greenblatt D. J., *Drug Metab. Dispos.*, **31**, 1125—1133 (2003).
31) Strassburg C. P., Kneip S., Topp J., Obermayer-Straub P., Barut A., Tukey R. H., Manns M. P., *J. Biol. Chem.*, **275**, 36164—36171 (2000).
32) Kagimoto M., Heim M., Kagimoto K., Zeugin T., Meyer U. A., *J. Biol. Chem.*, **265**, 17209—17214 (1990).
33) Gaedigk A., Blum M., Gaedigk R., Eichelbaum M., Meyer U. A., *Am. J. Hum. Genet.*, **48**, 943—950 (1991).
34) Honda M., Nozawa T., Igarashi N., Inoue H., Arakawa R., Ogura Y., Okabe H., Taguchi M., Hashimoto Y., *Biol. Pharm. Bull.*, **28**, 1476—1479 (2005).
35) Giessmann T., Modess C., Hecker U., Zschiesche M., Dazert P., Kunert-Keil C., Warzok R., Engel G., Weitschies W., Cascorbi I., Kroemer H. K., Siegmund W., *Clin. Pharmacol. Ther.*, **75**, 213—222 (2004).
36) De Mey C., Brendel E., Enterling D., *Br. J. Clin. Pharmacol.*, **29**, 486—490 (1990).
37) Kaijser M., Johnsson C., Zezina L., Backman U., Dimeny E., Fellstrom B., *Clin. Transplant.*, **11**, 577—581 (1997).
38) Bock K. W., Wiltfang J., Blume R., Ullrich D., Bircher J., *Eur. J. Clin. Pharmacol.*, **31**, 677—683 (1987).
39) Gallicano K. D., Sahai J., Shukla V. K., Seguin I., Pakuts A., Kwok D., Foster B. C., Cameron D. W., *Br. J. Clin. Pharmacol.*, **48**, 168—179 (1999).

Pravastatin Attenuates Left Ventricular Remodeling and Diastolic Dysfunction in Angiotensin II-Induced Hypertensive Mice

Zhujie Xu, MD, Hiroshi Okamoto, MD, PhD,* Masatoshi Akino, MD, PhD,* Hisao Onozuka, MD, PhD,* Yutaka Matsui, MD, PhD,† and Hiroyuki Tsutsui, MD, PhD**

Background: A substantial proportion of patients with heart failure have a normal ejection fraction and diastolic dysfunction. However, there are few data available to guide the therapy of these patients. The effects of statins on cardiac remodeling are well documented in animal models and it is reported that statin therapy revealed a survival benefit in patients with diastolic heart failure (DHF). However, the exact mechanisms of statins possibly explaining the decreased cardiovascular morbidity and mortality in patients with DHF have not been elucidated.

Methods: We used 8-week-old male C57BL/6J mice, in which angiotensin II was subcutaneously infused for 4 weeks to mimic cardiac remodeling and fibrosis. They were treated with either normal saline or pravastatin in daily doses, which did not lower the serum cholesterol levels and blood pressure.

Results: Pravastatin improved diastolic dysfunction in angiotensin II-induced hypertensive mice, which was associated with the amelioration of left ventricular hypertrophy and remodeling. However, statin treatment showed no effect on the increased systolic blood pressure or cholesterol levels by angiotensin II infusion. The cardioprotective effects of pravastatin were closely associated with the downregulation of collagen I, transforming growth factor-beta, matrix metalloproteinases-2 and -3, atrial natriuretic factor, interleukin-6, tumor necrosis factor-alpha, ROCK1 gene expression, and the upregulation of endothelial nitric oxide synthase gene expression.

Conclusions: The beneficial effects of pravastatin on DHF and structural remodeling are through cholesterol- independent mechanism of statins or "pleiotropic" effects of statins involving improving or restoring endothelial function and decreasing vascular inflammation. These findings suggest the potential involvement of ROCK1. Thus, treatment with pravastatin might be beneficial in patients with DHF.

Received for publication June 15, 2007; accepted September 10, 2007.

From the *Department of Cardiovascular Medicine, Graduate School of Medicine; and †Division of Molecular Immunology, Institute for Genetic Medicine, Hokkaido University, Sapporo, Japan.

Partly supported by the Ministry of Health, Labour and Welfare and Daiichi Sankyo Co., Ltd.

Reprints: Hiroshi Okamoto, MD, PhD, Department of Cardiovascular Medicine, Hokkaido University Graduate School of Medicine, Kita-15, Nishi-7, Kita-ku, Sapporo, 060-8638 Japan (e-mail: okamotoh@med.hokudai.ac.jp).

Copyright © 2008 by Lippincott Williams & Wilkins

Key Words: statins, diastolic heart failure, angiotensin II, fibrosis, remodeling

(*J Cardiovasc Pharmacol*™ 2008;51:62–70)

Diastolic heart failure (DHF) is a significant healthcare problem. Nearly 50% of all patients with chronic heart failure have diastolic dysfunction with high morbidity and mortality rates. On the other hand, there are few studies that provide any guidance or instruction in the treatment of this patient population. The pathophysiology and treatment of DHF is poorly understood. The hydroxymethylglutaryl-coenzyme A reductase inhibitors (statins), potent inhibitors of cholesterol biosynthesis, have been demonstrated beneficial in both the primary and secondary prevention of coronary heart disease. However, the overall clinical benefits observed with statin therapy appear that many of beneficial effects of stains on cardiovascular disease might extend beyond their effects on serum cholesterol levels.[1]

Indeed, recent experimental and clinical evidence indicates that some of the cholesterol-independent or "pleiotropic" effects of statins involve improving or restoring endothelial function, enhancing the stability of atherosclerotic plaques, and decreasing oxidative stress and vascular inflammation. Many of these pleiotropic effects of statins are mediated by their ability to block the synthesis of important isoprenoid intermediates, which serve as lipid attachments for a variety of intracellular signaling molecules. In particular, the inhibition of small GTP-binding proteins, Rho, Ras and Rac, whose proper membrane localization and function are dependent on isoprenylation, may play an important role in mediating the direct cellular effects of statins.[2] ROCK1 is the immediate downstream target of RhoA, which is also known as ROKβ and p160ROCK. Because ROCKs mediate various important cellular functions such as cell shape, motility, secretion, proliferation, and gene expression, it is likely that this pathway will intersect with other signaling pathways known to contribute to cardiovascular disease. Indeed, ROCKs have already been implicated in the regulation of vascular tone, proliferation, inflammation, and oxidative stress. However, it is not entirely clear how ROCKs are regulated, what some of their downstream targets are, and whether ROCK1 and ROCK2 mediate different cellular functions. There is growing evidence that the RhoA/ROCK pathway plays an important pathophysiological role in cardiovascular diseases and that inhibition of ROCKs by ROCK inhibitors or statins may be

beneficial. To date, a great number of cellular and physiological functions are mediated by ROCK, and ROCK activity is often elevated in disorders of the cardiovascular system. Clinically, inhibition of ROCK pathway is believed to contribute to some of the cardiovascular benefits of statin therapy that are independent of lipid lowering (ie, pleiotropic effects). Thus, inhibition of ROCK may be an attractive therapeutic target in reducing cardiovascular disease.[3] Indeed, ROCK1$^{+/-}$ haploinsufficient mice develop cardiac hypertrophy, but not fibrosis.[4] Similarly, in ROCK1-deficient (ROCK1$^{-/-}$) mice, the targeted deletion of ROCK1 protects the heart against pressure overload by inhibiting reactive fibrosis.[5] Therefore, the inhibition of ROCK1 in cardiomyocytes appears to play a predominant role in the prevention of cardiac remodeling and fibrosis.

Statins has been demonstrated to attenuate cardiac adverse remodeling by the prevention of cardiac fibrosis and hypertrophy.[6–8] Nonetheless, there have been no studies describing the role of Rho/ROCK pathway in attenuating diastolic dysfunction by statins. Thus, we investigated whether pravastatin could improve diastolic dysfunction in angiotensin II-induced cardiac hypertrophy mice through cholesterol-independent pathway and examined the role of ROCK1 in this process.

METHODS

Animals

Eight-week-old male C57BL/6J wild-type mice (n = 48) were purchased and given standard laboratory chow and tap water ad libitum. The mice were randomly divided into 4 groups and were treated over a 4-week period. Each of the four groups received the following treatment: oral normal saline and saline pump (Sal/Sal n = 8), oral pravastatin (Pra; 10 mg/kg per day) and saline pump (Pra/Sal n = 9), oral normal saline and angiotensin II (AII; 2 μg/kg per minute) pump (Sal/AII n = 15), and oral Pra (10 mg/kg day) and AII (2 μg/kg per minute) pump (Pra/AII n = 16). The mice were anesthetized with 0.01 mL/g of a mixture of ketamine and xylazine prior to subcutaneous placement of a miniosmotic pump (model 2004, Alza). The mice were fed either normal saline or pravastatin daily by means of gavage.

The dose of pravastatin was decided following a preliminary study, in which the minimum dose to reduce the cardiac fibrosis was selected for the present experiment. In the preliminary study, mice were under same experimental conditions as those in the present study. Eight-week-old male C57BL/6J wild type mice (n = 50) were randomly divided into 5 groups (n = 10/per group) and normal saline were infused with a mini-osmotic pump to Group I, angiotensin II (2 μg/kg per minute) were infused with a mini-osmotic pump to the other 4 groups over a 4-week period. Each of the five groups received the following treatment everyday by means of gavage: oral normal saline (Group I), saline (Group II), oral Pra (5 mg/kg per day; Group III), oral Pra (10 mg/kg per day; Group IV), and oral Pra (30 mg/kg per day; Group V). Compared with Group II, the minimum dose of pravastatin that significantly attenuated cardiac fibrosis (a value of $P < 0.05$ was considered statistically significant, and about 15% reduction in fibrosis) was selected for the following experiment.

In our study, all animal protocols were approved by our Institutional Animal Care and Use Committee.

Blood Pressure and Heart Rate

Before implantation of the pumps and at the end of this study, systolic blood pressure (SBP) and heart rate were measured in a conscious state in all mice using the indirect tail-cuff method (BP-98A, Softran, Tokyo, Japan) in a 37°C preheated cloth jacket for about 10 minutes. A minimum of 5 preliminary cycles were performed before collecting 10 measurements for each mouse. An average of such recordings was taken as the individual SBP and heart rate.

Echocardiography

Transthoracic echocardiography was performed using an EUB 8000 echocardiographic instrument (Hitachi-Medico, Tokyo, Japan). Mice were anesthetized by intraperitoneal injection with 0.01 mL/g of a mixture of ketamine (100 mg/kg) and xylazine (5 mg/kg). After removal of the thoracic fur, the mice were placed in a left decubital position on a feedback-controlled heating pad to maintain body temperature at 37°C. Doppler examinations were performed with a 13-MHz transducer using a baseline filter set at the lowest level. The 13-MHz-probe was prepared with a standoff built from the finger of a latex glove filled with ultrasound gel, which was centrifuged at 3000 rpm for 10 min to avoid air bubbles disturbing acoustical coupling. A smooth layer of 1.5–2.0 cm thick centrifuged ultrasound gel was placed on the chest of the mice and the probe was gently dipped into this layer of gel avoiding any pressure on the thorax to prevent thorax deformation or reflex bradycardia. Under the guidance of two-dimensional echocardiography, M-mode echocardiography was performed to measure the following parameters from the M-mode image of the left ventricle.[9] Posterior wall thickness (PW), end-diastolic (LVDd), and end-systolic left ventricular diameter (LVDs) were measured. Percent fractional shortening (%FS) was used to estimate the cardiac systolic function. It was calculated using the following formula: $\%FS = [(LVDd-LVDs)/LVDd] \times 100$.

The left lateral position was used to obtain an optimal Doppler image quality. The LV inflow tract was interrogated from the apical four-chamber view with the sample volume at the tips of the mitral leaflets. The E wave velocity (E/A) ratio and isovolumic relaxation time (IRT) were measured as estimates of the cardiac diastolic function. IRT was corrected by each R-wave and R-wave (RR) interval time to compensate for the heart rate variance, shown as c-IRT.

Myocardial Histopathology

After conducting in vivo hemodynamic studies, the heart was excised and dissected into the right ventricle and the left ventricle (LV), which included the septum. At that time, the whole heart and the LV were weighed. The LV was cut into 3 transverse sections: apex, middle ring, and base. The middle ring was fixed in 10% formalin and embedded in paraffin. Five-micrometer sections were cut and stained with Masson trichrome. Photomicrographs were processed with Adobe Photoshop software and then were quantified with NIH Image

© 2008 Lippincott Williams & Wilkins

software to measure the area of interstitial fibrosis and perivascular fibrosis, which were calculated as the ratio of the fibrosis area to the total area of the section field, which is photographed using a microscope and magnified and the ratio of the fibrosis area surrounding the vessel to the total vessel area. Twenty sections or about 40 vessels were examined in each heart, and results obtained in each group were averaged. To measure the myocyte cross-sectional area, each section was photographed using a microscope and magnified. Connective tissue and muscle areas were identified, and the profile margin of 30 to 40 myocytes cut into cross-sections was manually traced and digitized. The digitized profiles were transferred to a personal computer that calculated the area. Three to 4 fields were randomly selected from 2 to 3 coronal sections of each heart. Thus, about 100 to 200 myocytes were measured for each animal, and the mean myocyte cross-sectional area was calculated.[16]

Reverse-Transcription Polymerase Chain Reaction Analysis

The LV apex was snap-frozen in liquid nitrogen and stored at −80°C. Total mRNA was extracted and reverse-transcription (RT) polymerase chain reaction (PCR) was performed using specific primers for transforming growth factor (TGF)-β, collagen I, matrix metalloproteinases (MMP)-2 and -3, atrial natriuretic factor (ANF), endothelial nitric oxide synthase (eNOS), tumor necrosis factor (TNF)-α, interleukin (IL)-6, and ROCK1. Cycling conditions were 94°C for 30 seconds, 55°C for 30 seconds, and 72°C for 1 minute. PCR products were run on 2% agarose gel electrophoresis and exposed to ultraviolet light.

Real-Time Polymerase Chain Reaction

Total mRNA was extracted and real-time PCR was performed for the quantitative evaluation of TGFβ, collagen I, matrix metalloproteinases-2, -3 (MMP-2, 3), ANF, eNOS, TNF-α, IL-6 and ROCK1 gene expression. A sample of cDNA was diluted and mixed with 50 mL 2 × SYBR Green I and 0.3 μM of each primer. The mixture was loaded in a MicroAmp Optical 96-well plate. The first cycle of amplification was done at 95°C for 10 seconds. The next 40 cycles of amplification were done at 95°C for 5 seconds followed by 60°C for 33 seconds. PCR reactions were monitored in real time using an ABI Prism 7000 Sequence Detection System. Each sample was set up in triplicate. To control for reaction variation, all PCR results were normalized against glyceraldehydes-3-phosphate dehydrogenase (GAPDH) expression.

Western Blot Analysis of ROCK1

Tissue cytoplasmic protein was extracted from the base mass of the LV using NE-PER Nuclear and Cytoplasmic Extraction Reagents (Pierce, Rockford, IL). The aliquots were boiled for 3 minutes and then separated on sodium lauryl sulfate poly-acrylamide gel electrophoresis (SDS-PAGE) (10%). They were then transferred to a polyvinyliden difluoride (PVDF) membrane using a glycine buffer in the presence of 20% methanol. Antigen-antibody complexes were detected using ECL Plus Western Blotting Detection Reagents (Amersham Biosicences Inc.). The following primary antibodies were used: ROCK1 (AB3885, CHEMICON International, Inc.) and GAPDH (sc-25778, Santa Cruz Biotechnology, Inc.). The secondary antibody was sc-2004, a goat anti-rabbit immunoglobulin G, horseradish peroxidase (HRP) conjugate.

Plasma Biochemical Measurement

Before euthanization, artery blood samples (1 mL) were collected to determine plasma total cholesterol and low-density lipoprotein (LDL) cholesterol levels.

Statistical Analysis

All results are expressed as the mean ± SEM. Multiple comparisons among 3 or more groups were performed by 2-way analysis of variance and Fisher exact test for post-hoc analyses. A value of $P < 0.05$ was considered statistically significant.

TABLE 1. Body Weight, Systolic Blood Pressure, Total Cholesterol, and LDL Cholesterol

Parameter	Sal/Sal	Pra/Sal	Sal/AII	Pra/AII
n	8	9	15	16
Body weight (g)				
Baseline	22.6 ± 0.6	22.2 ± 0.6	22.6 ± 0.4	22.4 ± 0.3
At 4 weeks	24.3 ± 0.8	25.8 ± 0.7	23.4 ± 0.4	24.3 ± 0.6
SBP (mm Hg)				
Baseline	111.5 ± 1.6	113.5 ± 1.5	110.6 ± 1.9	117.1 ± 2.7
At 4 weeks	118.7 ± 1.1	115.3 ± 1.6	133.3 ± 2.3*	139.6 ± 2.3*
LVW/BW (mg/g)				
	2.8 ± 0.1	2.6 ± 0.1	4.2 ± 0.2*	3.7 ± 0.1*†
Heart rate (bpm)	629 ± 11	639 ± 10	646 ± 8	629 ± 11
Total cholesterol (mg/dL)	73.00 ± 5.78	77.22 ± 6.58	109.45 ± 21.22*	111.65 ± 5.85*
LDL cholesterol (mg/dL)	10.08 ± 1.44	13.32 ± 4.08	21.86 ± 2.46*	19.87 ± 4.35*

Values are means ± SEM.
LVW/BW, left ventricle weight/body weight.
*$P < 0.05$ vs. Sal/Sal and Pra/Sal.
†$P < 0.05$ vs. Sal/AII.

© 2008 Lippincott Williams & Wilkins

TABLE 2. Echocardiograph Measurements 4 Weeks After Treatment

Parameter	Sal/Sal	Pra/Sal	Sal/AII	Pra/AII
Posterior wall thickness (mm)	0.56 ± 0.09	0.57 ± 0.03	0.69 ± 0.12*	0.63 ± 0.09
Left ventricular dimension diastole (mm)	4.29 ± 0.10	4.27 ± 0.32	4.20 ± 0.29	4.23 ± 0.26
Left ventricular dimension systole (mm)	2.55 ± 0.15	2.57 ± 0.20	2.73 ± 0.28	2.80 ± 0.21
Fractional shortening (%)	38.86 ± 2.17	38.27 ± 3.10	36.38 ± 3.56	36.72 ± 2.83
E wave velocity ratio	2.628 ± 0.122	2.741 ± 0.661	2.208 ± 0.166*	2.533 ± 0.300†
Corrected-isovolumic relaxation time (ms)	0.107 ± 0.014	0.109 ± 0.026	0.147 ± 0.013*	0.114 ± 0.019†

Values are means ± SEM.
*$P < 0.05$ vs. Sal/Sal and Pra/Sal.
†$P < 0.05$ vs. Sal/AII.

RESULTS

Effects on Blood Pressure, Heart Rate, and Cholesterol

The effects of statin treatment on SBP, heart rate, and cholesterol are summarized in Table 1. Before treatment, there were no significant differences among the 4 groups. After 4 weeks, AII infusion significantly elevated both the SBP and cholesterol levels. Pravastatin treatment had no effect on these changes.

Effects on Cardiac Function

To investigate cardiac function, we performed an echocardiogram. The results of the examination are shown

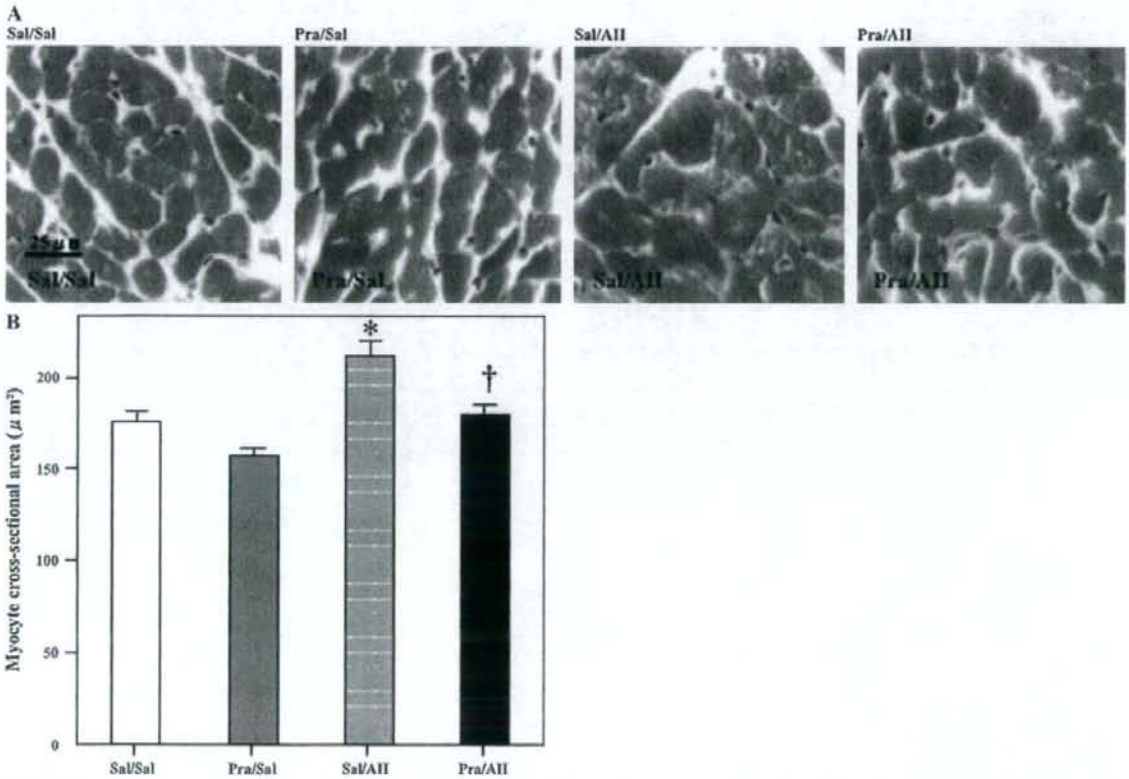

FIGURE 1. Cardiac myocyte cross-sectional area in mice. A, Representative cross-sections of cardiomyocytes stained with Masson's trichrome. Scale bar, 25 μm. B, Bar graph shows quantitative analysis of cardiac myocyte cross-sectional area (μm^2). Values are means ± SEM (Sal/Sal: n = 8, Pra/Sal: n = 9, Sal/AII: n = 15, Pra/AII: n = 16). *$P < 0.05$ vs. Sal/Sal and Pra/Sal; †$P < 0.05$ vs. Sal/AII.

© 2008 Lippincott Williams & Wilkins